A novel liquid nitrogen fill level meter for the AGATA triple cluster detector

Diplomarbeit von: Daniel Lersch
Unter der Leitung von: Prof. Dr. Peter Reiter

Institut für Kernphysik der Universität zu Köln

Dezember 2009

Contents

1 Introduction **1**

2 The AGATA-spectrometer **3**
2.1 The AGATA-triple-cluster 4
2.1.1 The AGATA-capsule 4
2.1.2 The cryostat 6
2.2 The cryogenic lling system 8

3 The LN_2-monitor **11**
3.1 Cooling with liquid nitrogen 11
3.1.1 Characteristics of a semiconductor 11
3.1.2 Working under vacuum 13
3.1.3 The AGATA-dewar 15
3.2 Temperature-monitoring 15
3.2.1 The PT-100-sensor 15
3.2.2 The Bias-shut-down 17
3.3 The capacitiveLN_2-read-out (I) 19
3.3.1 The steady state and vertical dewar-postion 19
3.3.2 Measuring device (I) 21
3.3.3 Cooling-in- and warming-up-process 23

4 LN_2-consumption-measurements **29**
4.1 LN_2-consumption of ATC(2) 29
4.1.1 Setting up ATC(2) 29
4.1.2 Results: ATC(2) 30
4.2 LN_2-consumption of ATC(3): The capton-cable-test 32
4.2.1 Setting up ATC(3) 33
4.2.2 Results: ATC(3) 33
4.2.3 Vacuum-leak in ATC(3) 34
4.3 LN_2-consumption of ATC(4) 35
4.3.1 Setting up ATC(4) 36
4.3.2 Cooling-in ATC(4) 38
4.3.3 Results of the consumption tests 39

5 The LN_2-read-out (II): A capacitive preamplifier **41**
5.1 The capacitive preampli er 42
5.1.1 The CAV414 44
5.1.2 Further signal processing 47
5.1.3 First tests with the prototype 47
5.2 The LN_2-read-out-box 49
5.2.1 Characterising theLN_2-read-out 49

5.2.2 Calibrating the LN_2-read-out 51

6 Position-dependence of the LN_2-monitoring 55
6.1 In uence of horizontal inclination and axial rotations 56
6.1.1 Calculations of S( ) and V( ) of a liquid inside a cylinder for di erent inclination 57
6.1.2 In uence of the dewars geometry 62
6.1.3 Axial rotations 62
6.1.4 Simulating the time behaviour of the capacity C(t) . . . 62
6.2 Position-dependent measurements (I) 63
6.3 Position-dependent measurements (II) 67
6.4 First summary and discussion of the results 70

7 Summary and outlook 73

A Warming-up-process 75

B Consumption measurements 76
B.1 Measured capacities and lling heights during the consumption measurements of ATC(2) 76
B.2 The capton-cable-test 79
B.2.1 Measured capacities and lling heights during the consumption measurements of ATC(3) 79
B.2.2 LN_2-consumption calculated by the measured lling heights 79
B.3 LN_2-consumption and operation time of ATC(4) after a cooling-in-process 81
B.4 Measured lling capacity as a function of time for di erent loads at ATC(4) 81

C The C/V-transcenducer 85
C.1 Pin out and component placement speci cation of the CAV414 . 85
C.2 Increasing and decreasing the gain 85
C.3 Measuring U_0, U_{max} and G_{max} for box 1,3 and 4 87

D Simulation of S( ) and V( ) 90
D.1 The correction terms S_{wdg} and V_{wdg} 90
D.2 Simulation of S and V for a constant volume V 91
D.3 Simulation of S and V for a re lled dewar 94
D.4 Simulating the lling capacity C(t) 95
D.5 Measured lling capacity as a function of the inclination for a given lling height 97

Chapter 1

Introduction

High resolution -spectroscopy is the underlying method to investigate excited stats in nuclei and to understand nuclear structure physics. Since the complexity of nuclear structure experiments is still increasing, the requirements on an e ciently and accurately working -spectrometer are considerably high.
AGATA (Advanced GAmma Tracking Array) is an European project to establish a new -spectrometer which is based on modern electronics with the encapsulated, highly segmented germanium-crystal-technology. A characteristic of these complex detector-systems is the continuous operation at liquid nitrogen temperature. A lack of cooling would cause a severe damage of these delicate detectors and major losses in operation time and nancial losses would be related to such a warmup event. Therefore the determination of the liquid nitrogen consumption and the direct monitoring of the liquid nitrogen level inside the detector are of great importance.
The subject of this thesis is a novel liquid nitrogen ll level meter for the AGATA-triple-cluster detectors. The consumption of liquid nitrogen depending on di erent setups of the AGATA-detector is investigated with the newly developed device.
Due to various AGATA detector positions the a ect of the consumption of liquid nitrogen and the in uence on the liquid-nitrogen-level-read-out itself was subject of this thesis.

Chapter 2

The AGATA-spectrometer

The AGATA-spectrometer is designed as 4 -spectrometer and will consist of 60 antisymmetric triple cluster (ATC) detectors (see g. 2.1) in its nal con guration. Each cluster contains three 36-fold-segmented, encapsulated high purity n-type Germanium (HPGe) crystals [DB01]. The geometry of the

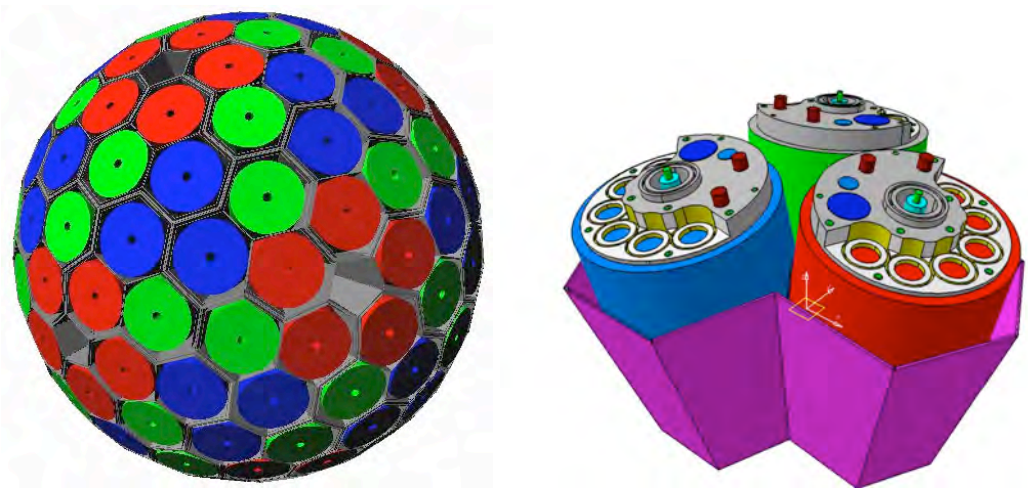

Figure 2.1: Left: Drawing of the AGATA-array consisting of 180 hexagonal shaped crystals. The inner radius of the shell is 23.5 cm [JE08], as 82 % of the solid angle are covered by the Ge-crystals. The total amount of germanium needed for this con guration is 362 kg [JE08]. Right: The Ge-crystals inside one triple cluster are not shaped symmetrically, three di erent asymmetric types are used instead: A-type (red), B-type (green) and C-type (blue).

AGATA-array is determined by the following requirements [DB01]:

- Full energy e ciency and spectral response for -rays in the energy range from 10 keV to 10 MeV
- Symmetry of the con guration
- Modularity
- Available inner space (inner radius of shell)
- Amount of germanium used (cost)

The nal design of the array is shown in g. 2.1. The AGATA-spectrometer will be used for several types of experiments which are characterised by a

-radiation after a reaction zone. Thus a spherical con guration of the Ge-crystals around a target provides the highest detection e ciency [DB01]. Many methods of -spectroscopy (e.g angular distribution, correlation measurements etc.) take advantages of a symmetric arrangement of the detectors which is given by the con guration shown in g. 2.1 [DB01]. In order to realise a full solid angle coverage in a spherical arrangement, the detectors are shaped asymmetrically.
Figure 2.1 displays the predicted performance for the future AGATA-spectrometer at energies of 1 MeV. The e ciency for a single -particle is determined by the amount of detection material which surrounds the radiation source [DB01]. -rays with energy $E = 1$ MeV for example are detected with an e ciency of 43.3 %. According to the attenuation law $I = I_0 e^{-x}$ for gamma rays, the thickness of the surrounding Ge-material becomes more important for higher -energies [DB01]. If the -multiplicity M increases then the number of detecting elements has to increase too, in order to distinguish between di erent -rays. Considering this, simulations have shown that 6000 8000 detection elements are required which is realised by 6660 channels for the AGATA-spectrometer. The peak-to-total ratio $P=T$ describes the spherical response of

Multiplicity	1	10	20	30
E ciency [%]	43.3	33.9	30.5	28.1
Peak to total ratio [%]	58.2	52.9	50.9	49.1

Table 2.1: Predicted performance of 180 triple cluster detectors in the AGATA for -energies of 1 MeV [JE08].

the detector. A high position resolution is assured by the segmentation of the Ge-crystals, as the segments are su ciently small [DB01].

2.1 The AGATA-triple-cluster

Each AGATA-triple cluster (see g. 2.4) consists of two main parts: on the one hand the Ge-crystals which are detecting the -rays and the cryostat on the other hand. The cryostat connects the crystals with the high front end read-out-electronics and keeps the crystals at an temperature near 196 C since they are cooled with liquid nitrogen.

2.1.1 The AGATA-capsule

The high angular resolution and position sensitivity of the AGATA-spectrometer is related to the fact that all Ge-crystals in the array are segmented. Each Ge-crystal comprises 36 segment-electrodes and one core-electrode. In order to separate the delicate Ge-crystals from the cryostat and to protect them during repairs of the electronics, all crystals are encapsulated. Figure 2.2 shows an

Figure 2.2: Left: CAD-drawing of an encapsulated, segmented hexagonal Ge-crystal [DB01]. Middle: Labeling of the segmented detector: The rows are labelled from 1 to 6, as no. 6 is the upper segment. The rings are labelled from A to F. Right: Photograph of an AGATA-detector. In order to read out the signals of the segments a board is mounted on top of the crystal which connects the first preamplifier stage with the segments.

encapsulated AGATA-detector with a board mounted on top. The capsules are made of aluminium with a 8 mm wall thickness. The space between the detector and the Al-caspule is about 0.5 mm. The whole detector has a weight of 2 kg.
The AGATA-capsules are manufactured by the company Canberra, Lingolsheim (Strasbourg), France. Before these crystals are mounted in the AGATA triple cryostat, they have to pass a customer acceptance test (CAT) which is done at IKP (Institut für Kernphysik) Cologne. The results of such a test are displayed in Fig. 2.3. All segments and the core of this detector are performing well. The FWHM of segment B3 for example is 1 keV for a γ-energy $E_\gamma = 59.6$ keV.

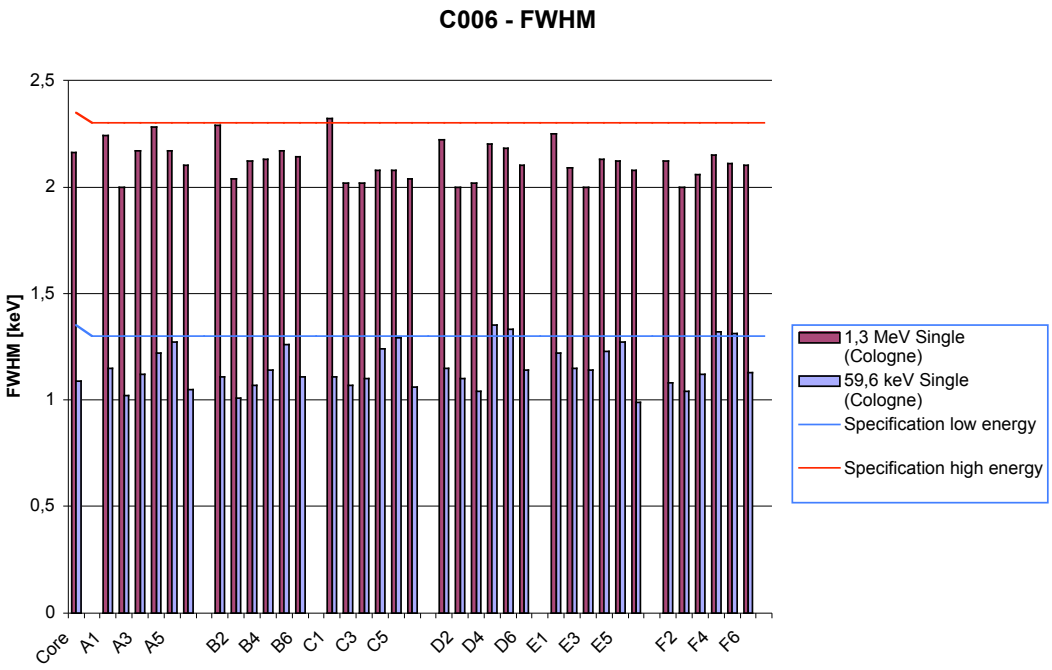

Figure 2.3: Results of a customer acceptance test done at IKP Cologne for an asymmetric C-type AGATA-detector. The full width at half maximum (FWHM) of a measured energy peak is speci ed for the segments and the core. The speci cations for the segments are:1:3 keV for an energy of59:6 keV, 2:3 keV for 1:3 MeV and for the core: 1:35 keV at 122 keV, 2:35 keV at 1:3 MeV. The measured FWHM of the segments and core of this detector are performing well within the speci cations.

2.1.2 The cryostat

Each AGATA-cryostat (see g. 2.4) may in principle be divided in three main sections:

1. The cold part: Three asymmetric, hexagonal, encapsulated Ge-crystals and the rst amplifying stage are operated under a high vacuum of < 10^{-7} mbar and a temperature near 196 C. The cold part is covered by an aluminium endcap with a length of27:5 cm and a weight of420 g

2. The warm part: The warm preampli ers are connected by feedthroughs with the amplifying stage in the cold part. The ampli ers in the cold and warm part are operated with a low-voltage of 6 V and 12 V.

3. The liquid nitrogen is hosted inside a dewar.

Since all AGATA-detectors are cooled withLN_2, the dewar is linked by a cooling nger with the cold part (see chapter 3) where the crystals are attached. The whole cryostat has a total length of92 cm, as the dewar has a length of 38 cm. The total weight of the cryostat without liquid nitrogen inside is38 kg. Figure 2.4 shows a symmetric triple cluster where symmetric detectors are mounted inside. But the working principle is identical to that of an asymmetric triple cluster.

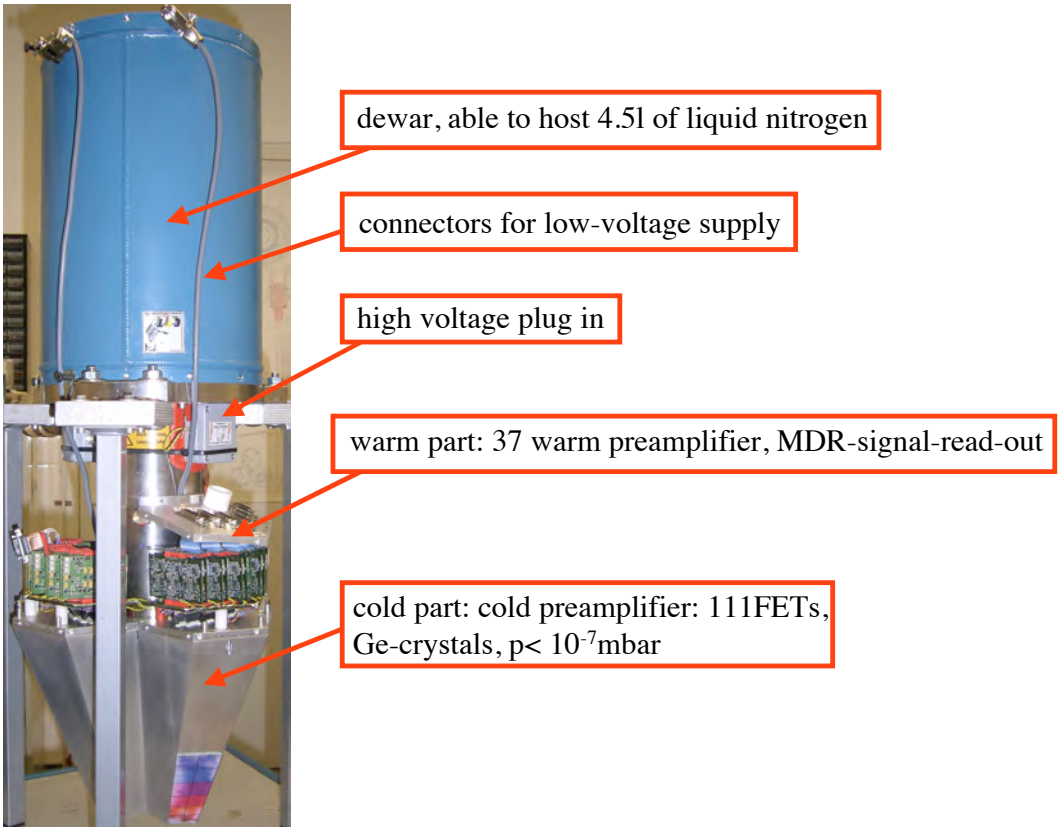

Figure 2.4: Symmetric AGATA-triple-cluster (STC) at IKP Cologne. The only di erence between a symmetric and an asymmetric triple cluster is given by the shape of the detectors and the endcap. The amplifying stage in the cold part comprises 111 (3 36 segments+ 3 cores) feld-e ect-transistors (FETs). The signals coming from the cold part pass the warm preampli ers (2 warm preampli er provide six segments, whereas each core-signal is read out by one warm preampli!er 37 warm preampli ers in total) and are read out by a MDR-cable afterwards.

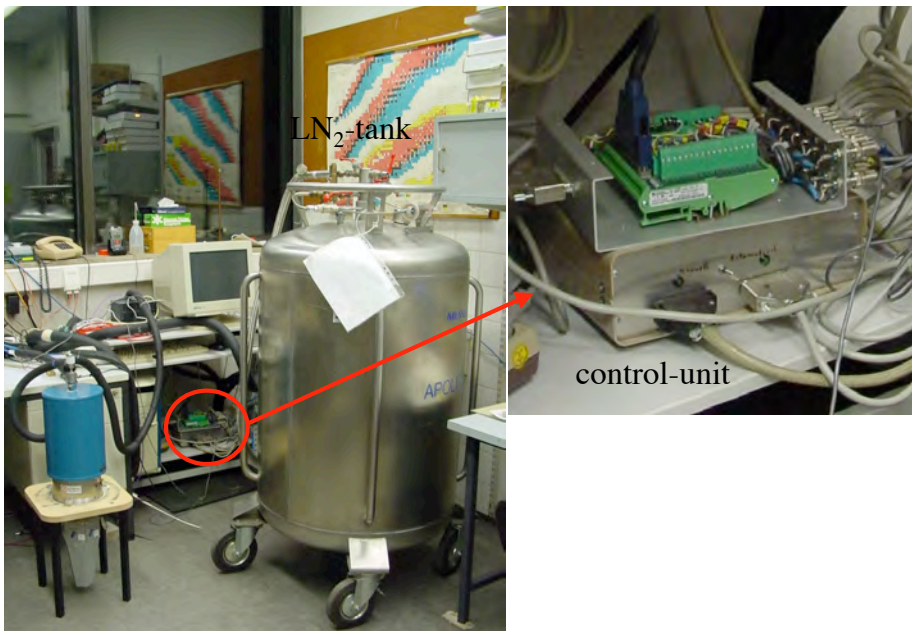

Figure 2.5: Automatic cryogenic lling system at IKP Cologne. The LN_2-tank is able to host 450 l of liquid nitrogen and linked by a valve with the control unit. The control unit itself is linked to a PC where the start of a lling and the lling period are adjusted. The control unit drives several valves which are connected by lling-nozzles with the detectors. Each lling-nozzle is equipped with an over ow, as the over ow itself is controlled by a PT100-sensor. If this sensor detects a temperature of 196 C the control unit shuts the valve and the lling is terminated. The adjusted lling period of the Cologne- lling-system is 8 h. The liquid nitrogen is lled with a pressure of 1.5 2 bar into the dewar. The duration of the lling for an AGATA-triple dewar varies between 5 12 min depending on the pressure inside the tank.

2.2 The cryogenic lling system

All detectors in the AGATA-array are linked to an automatic cryogenic lling system which provides every cluster with liquid nitrogen. The requirements to such an automatic lling system are:

Reliability

The lling should start automatically at a given point in time and end automatically when a certain liquid nitrogen level inside the dewar is reached.

A warning signal has to be sent out by the system if the lling is somehow interrupted or impeded.

A force lling has to be done in the case the regular lling is interrupted or the detectors is warming up above a temperature treshold.

Figure 2.5 shows the automatic cryogenic lling system which is used in Cologne. The control unit is driven by a Linux-PC which is connected to the Internet. If a lling process was successful (or not) an email is sent out. The reliability of this system depends strongly on the pressure inside the LN_2-tank. Thus it is of great importance that the tank is equipped with a self-adjusting pressure unit which keeps the pressure always at a constant level. The Cologne- lling-system

is able to provide two AGATA-trilpe-clusters and one AGATA-single-detector at once with liquid nitrogen.
The lling-system for the AGATA-array is more complex but mainly working in the same way. Figure 2.6 displays the general layout of a cryogenic system at the LNL (Laboratori Nazionali di Legnaro) in Legnaro. The liquid nitrogen is hosted in the outer tank which is connected by a pipeline with the detectors. Each detector is equipped with a gas-exhaust. The nitrogen gas is collected in a vessel (lime-green coloured box) which is equipped with a PT100-sensor and connected to the out ow watchdog. If the gas becomes liquid the PT100 sensor at the vessel gives a signal to the watchdog which stops the lling automatically [Koj07]. Each detector has an extra PT100-sensor (DPT) which

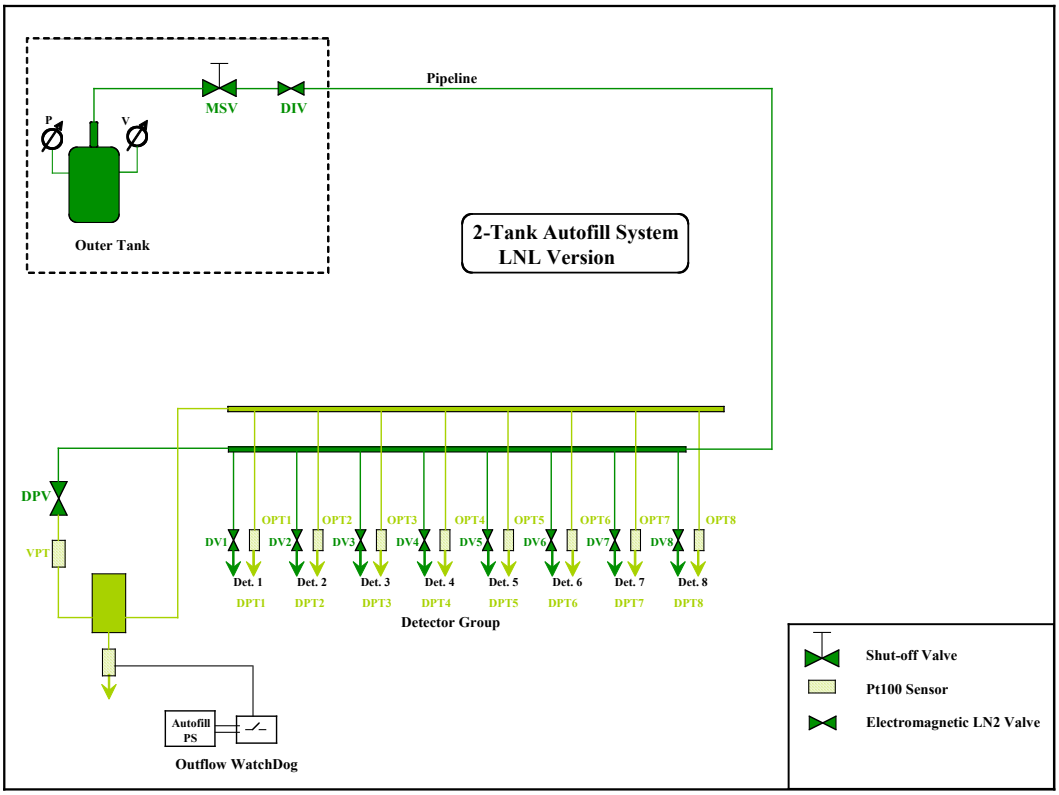

Figure 2.6: General structure of the cryogenic system at Legnaro [Koj07]

monitors its temperature. In the case that the temperature exceeds a certain value the detector valve (DV) opens and the DPT gives a signal to the watchdog and a force- ll is done. Due to the complexity of such a system it is not unlikely that a failure may occur and prevent the automatic lling which would be crucial for any detector in the array. A missing liquid nitrogen ll causes an uncontrolled warming up of the detector. This leads to an overheating of the crystals while they are operated under high voltage. Moreover the electronics inside the cold part might be damaged by high voltage sparks.
Thus an independent liquid nitrogen monitor is a necessary extension of the control system. The new monitor is directly linked to the liquid nitrogen level inside the dewar. In case the LN_2-level falls below a certain value, the monitor will cause a force- ll. The working principle of such a LN_2-monitor and the di erence with respect to a PT100-sensor inside the detector is discussed in the following section.

Chapter 3

The LN_2-monitor

The AGATA-detectors have to be kept at a low temperature 190 C and monitoring of the LN_2-level is of great importance. In this chapter the basic concepts and prerequisites of the new LN_2 monitor are introduced.

3.1 Cooling with liquid nitrogen

The detectors used for the AGATA-triple-clusters are 36-fold segmented high purity germanium detectors. Germanium is a chemical element of the fourth main group and thus is a semiconductor which has a temperature dependent conductivity. The electrical conductivity $_{el}$ inside a semiconductor depends on the **intrinsic carrier concentration** $n_i(T)$ [EH05]:

$$_{el} \quad n_i(T) \tag{3.1}$$

The temperature dependency of n_i determines the conductivity and is discussed in the following section.

3.1.1 Characteristics of a semiconductor

A solid is characterised as conductor, semiconductor or isolator by the bandgap $E_g = E_c \quad E_v$ between the valence band and conduction band (see g. 3.1 left). Considering a semiconductor the bandgap is in a region of $E_g = 0{:}5$ 1 eV [Dem05]. The probability that an electron inside a solid occupies a state with energy E at a given temperature T is described by the **Fermi-Dirac-distribution** [Dem05]:

$$f(E) = \left[\exp\left[\frac{(E \quad E_F)}{k_B T}\right] + 1 \right]^{1} \tag{3.2}$$

As E_F is the Fermi-energy. A plot of equation 3.2 is shown on the right hand side of g. 3.1. If the temperature T of the system is 0, no state with energy $E > E_F$ can be occupied by electrons. When temperature is nite, states with energies $E > E_F$ may be occupied. Therefore for a certain temperature T the probability exists that an electron inside a semiconductor may transcendent through E_g into the conduction band. The electrical conductivity of a solid is determined by the concentration n of electrons in the conduction band which is given by: [Kit06]

$$n = \int_{E_c}^{1} {}_e(E) \quad f(E)dE \tag{3.3}$$

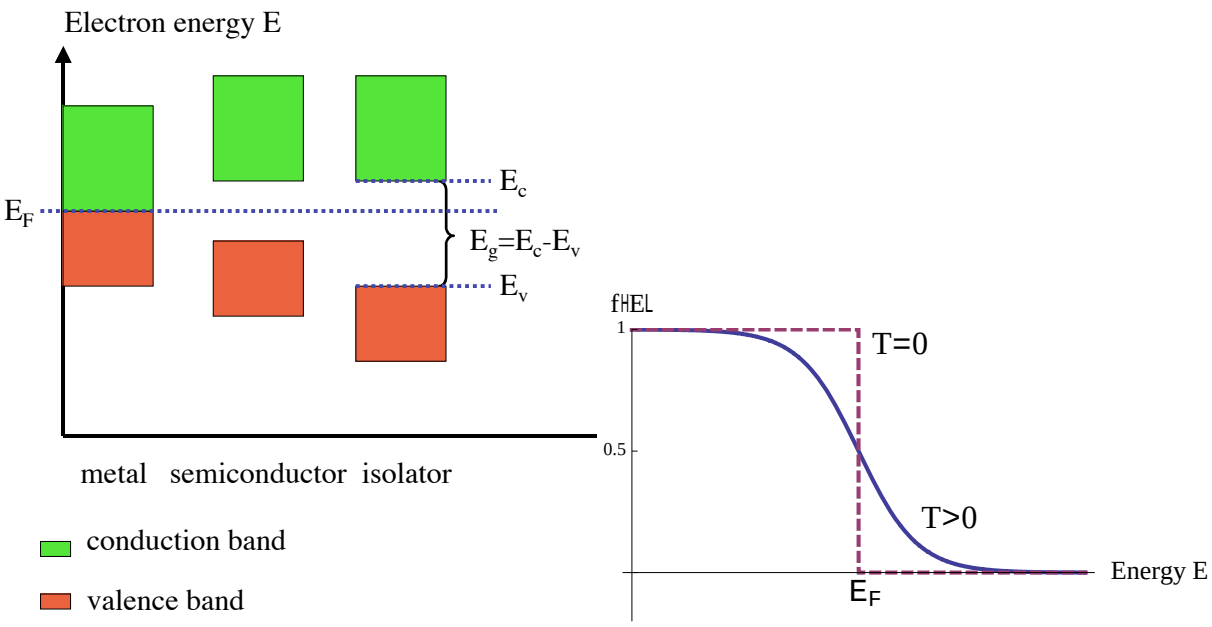

Figure 3.1: Left: Schematic drawing of the band model for solids. The conduction band has a minimum energy E_c whereas the valence band has a maximum energy E_v [Dem05]. The energy E_F is the Fermi-energy and denotes the highest energy state at $T = 0$ which is still occupied with electrons [Dem05]. Right: Plot of the Fermi-Dirac-distribution $f(E)$ as a function of the energy E. If the energy is $E = E_F$, the distribution takes the value $f(E_F) = 0.5$. For the temperature $T = 0$ the distribution is equal to the -function.

As $_e$ is the density of states for electrons and $f(E)$ the Fermi-Dirac-distribution [Kit06]. Each electron in the conduction band causes a positive charge called hole in the valence band. Referring to equation 3.3 the concentration of holes in the valence band is given by [Kit06]:

$$p = \int_{1}^{E_v} {}_h(E) \; f_h(E)dE \qquad (3.4)$$

$_h$ describes the density of states for holes and $f_h(E) = 1 \quad f(E)$ [Kit06] the corresponding distribution. The temperature dependent intrinsic carrier concentration is then given by [EH05]:

$$n_i(T) = \sqrt{n \; p} = n_{i0} \; T^{3=2} \; \exp\left(\frac{E_g}{2k_B T}\right) \qquad (3.5)$$

Considering germanium for example, the bandgap is $E_g = 0.66$ eV and $n_{i0} = 1.57 \; 10^{15}$ cm ^{3}K $^{3=2}$ [EH05]. Equation 3.4 is shown in gure 3.2, where $\log[n_i]$ is plottetd with respect to the inverse temperature $1=T$. For high temperatures the charge carrier concentration is considerably high. In order to measure only electron-hole-pairs created by radiation, the semiconductor has to be kept at low temperature: $T \quad 98$K. The most common cooling techniques applicable are:

1. Cooling with liquid nitrogen LN_2
2. Cooling with liquid helium

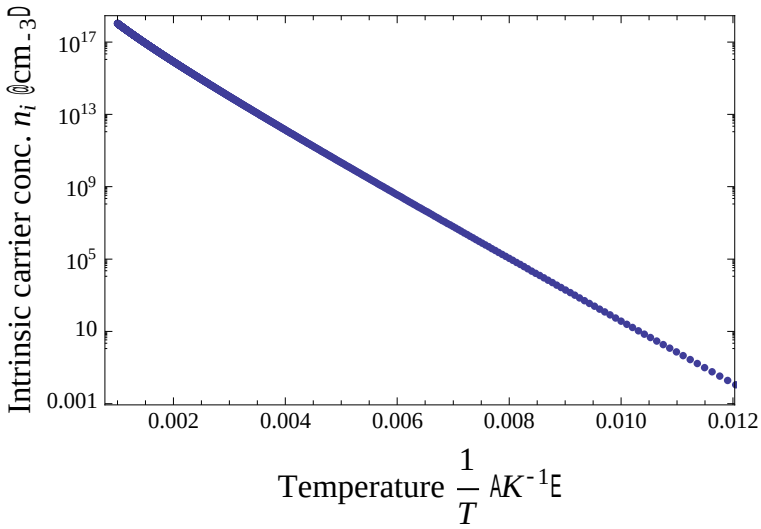

Figure 3.2: The intrinsic carrier concentration $n_i(T)$ plotted for germanium with respect to the temperature T.

3. Cooling with liquid argon

The AGATA-triple-clusters are cooled with liquid nitrogen which is hosted in a dewar (see g. 3.5). The dewar itself is linked by a cooling nger with the germanium crystals, as they have a temperature about 190 C when being cooled. This temperature is in a region where the intrinsic carrier concentration is marginal (see g. 3.2) and thus does not contribute to the concentration of charges which are created by radiation. In order to keep this temperature at a constant level the crystals environment needs to be evacuated. Otherwise the gas between the crystals and the endcap causes a thermal contact to the outside environment of the cryostat which leads to a heating of the crystals.

3.1.2 Working under vacuum

All AGATA-detector-systems are operated under high vacuum (p (7 10 ^{7} mbar), which means the crystals and electronics inside the cold part are evacuated. Operating the cluster under such a vacuum has two main aspects:

i) The radiation detection only works if the germanium crystals are kept at a low temperature and therefore a thermal contact between them and the cryostat needs to be avoided.

ii) If the cluster is not operated under vacuum, spontaneous discharges may occur and cause a severe damage of the electronics inside the cold part.

The second aspect is related to the **Paschen-law** which is displayed in g. 3.3. If a voltage is applied to two electrodes in a gaseous environment, free electrons get accelerated and scatter with the gas molecules. This scattering causes an ionization or excitation of the molecules which leads to more free electrons [Rai99]. These free electrons can ionize further molecules. Whether this chain reaction stops or causes an avalanche of free electrons depends on the pressure p of the gas, the distance d between the electrodes and the applied voltage U. In case of an avalanche of free electrons, a current may occur which may cause a severe damage of an electrical system. The relation between the

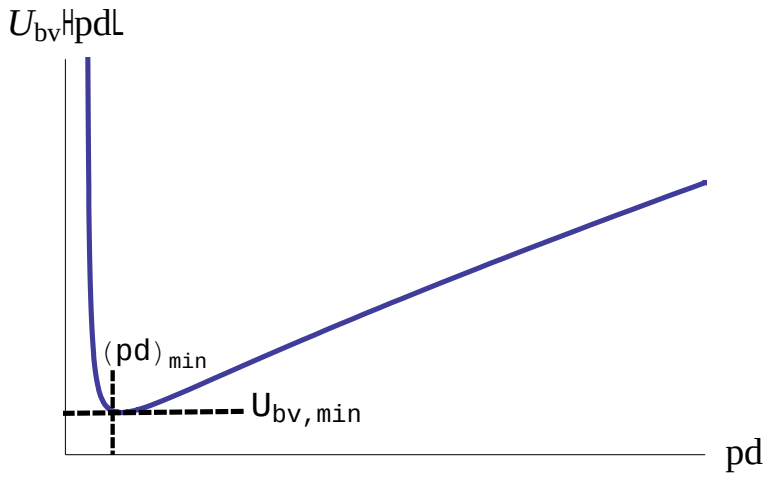

Figure 3.3: Paschen-curve of the breakdown U_{bv}(pd) with respect to the product of pressure and distance pd. The minimum voltage $U_{bv;min}$ is indicated by the black dashed lines.

breakdown voltage U_{bv} which causes the severe current and the product of p and d was found by Friedrich Paschen [pas09]:

$$U_{bv} = \frac{c_1 \quad pd}{\log[c_2 pd] \quad \log[\log[1 + \quad ^{1}]]} \tag{3.6}$$

The constants c_1 and c_2 depend on the gas between the electrodes and the electrode material itself. is called the Townsend-coe cient [Rai99] and determines whether an avalanche is formed or not. The breakdown voltage is minimal if the product of pressure and distance takes the value (pd)$_{min}$ (see g. 3.3). If pd < (pd)$_{min}$, the gas pressure is too low and the distance between the electrodes too short the probability for a scattering between the free electrons and gas molecules decreases. Thus a higher voltage for creating avalanches is needed. For values which are larger than (pd)$_{min}$ (see g. 3.3) the breakdown voltage depends linear on the product of pressure and distance [Rai99]:

$$U_{bv} \quad pd; \; pd > (pd)_{min} \tag{3.7}$$

High pressure forces the electrons to scatter with the molecules before they have enough energy to ionize or excite them. Large distances between the electrodes will cause a weak electrical eld if the voltage is not increased. Thus the electrons gain not enough energy to ionize the gas molecules. Fig. 3.4 shows three di erent Paschen-curves for three di erent gases, e.g air with a pressure of 10 Torr 13 mbar and a distance of 1 cm causes a break down voltage of U_{bv} 10^3 V. This value is crucial for any AGATA-detector since the operational voltage is 4 5kV. In order to achieve a high breakdown voltage which is not in the range of the operational voltage, a low pressure or high vacuum is needed. A special feature of the AGATA-cryostats are the getter inside them which have the ability to bind gas molecules [Rot79]. The getter used in AGATA-cryostats work in a low temperature environment, which can be reached by using LN_2. The getter start binding gas molecules when a certain (low) temperature T_l is reached which happens during a cooling-in-process of the cryostat. When the pressure of 10^{7} mbar is reached it will remain inside the cryostat as long as the temperature T inside the cryostat is:

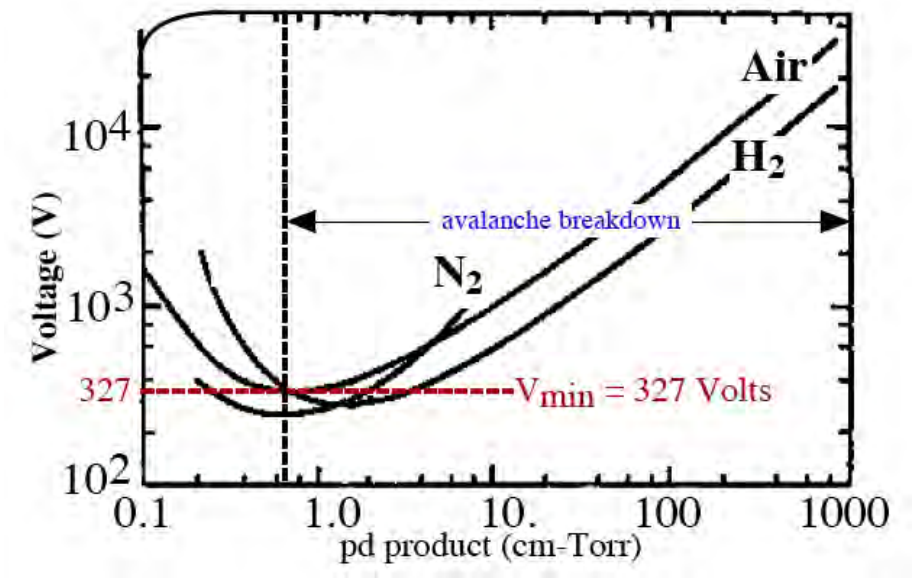

Figure 3.4: Plot of equation 3.5 for three di erent gases: air, N_2 and H_2 [Cob41].

$T < T_l$. When the temperature inside the cryostat is above T_l the getter start gasing out immediately and the pressure increases. According to Paschen's law a spontaneous discharge may occur and damage the electronics. Thus there is a need for constant cooling and a stable monitoring of the LN_2-level inside the dewar. In the following sections two oportunities of temperature- / LN_2-monitoring will be discussed.

3.1.3 The AGATA-dewar

Figure 3.5 shows an AGATA-triple-cryostat and a schematic drawing of an AGATA dewar where the liquid nitrogen is hosted. The germanium crystals are in thermal contact with the dewar through a copper cooling nger. An AGATA dewar is able to host 4.5 l of liquid nitrogen which is roughly the half of the dewars volume. The dewar has a total length of l = 38 cm and an outer diameter d = 25 cm and is equipped with a pressure control valve which opens automatically if the pressure inside the dewar is about 1.0 bar. A possibility to check the LN_2-level inside the dewar is to open the valve and measure the lling-level manually. But this method is too ine cient because the AGATA-array consists of 60 triple cluster which have di erent positions inside the array and no digital data produced to be used on a PC.

3.2 Temperature-monitoring

The LN_2 lling level can be indirectly checked by monitoring the temperature inside the dewar and the temperature of the germanium crystals. If the crystals are not cooled anymore their temperature will increase.

3.2.1 The PT-100-sensor

A most common possibility of monitoring the temperature inside the dewar is using a PT-100 sensor. Such a sensor consists of a PT-resistance $R(T)$, which

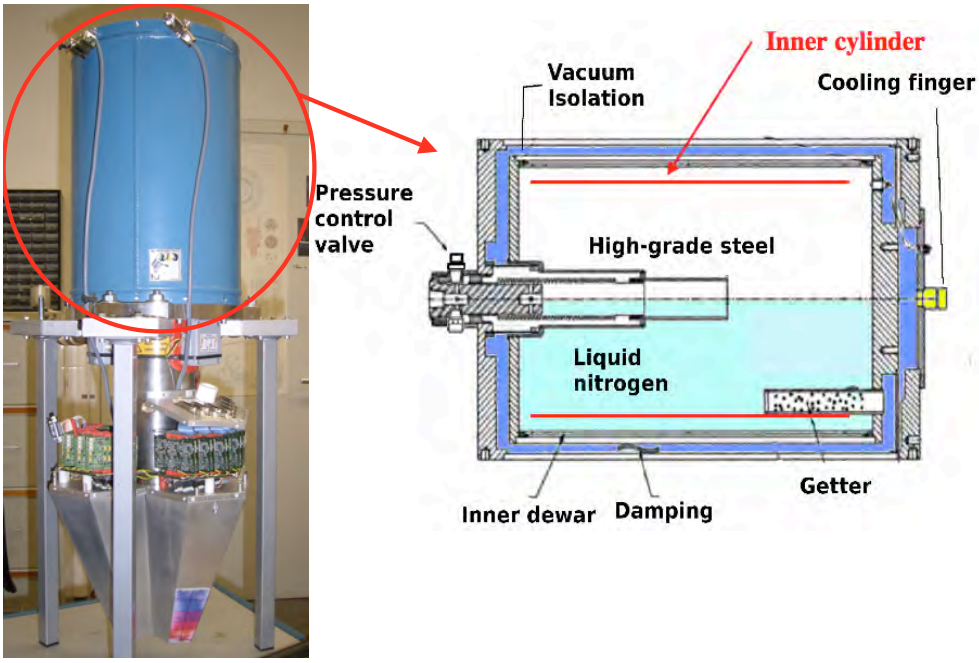

Figure 3.5: Left: AGATA-Triple-cryostat at IKP-Cologne. The blue part on top is the dewar where the liquid nitrogen is hosted. Right: Schematic drawing of a dewar used for AGATA. The dewar is linked to the crystals by a cooling nger. A getter is mounted inside the dewar to hold the pressure low. The interior of the dewar is separated from the exterior by a damping and a vacuum isolation as the vacuum region inside the dewar is indicated in dark blue. The inner metallic cylinder (indicated by the red lines) is used for the LN_2-monitoring. The lling nozzle extends about one half into the inside of the dewar. Thus the maximum lling height is limited by the length of the lling nozzle.

varies as function of the temperature T. For low temperatures $T \quad 0\ C$ the resistivity is described by [pt1]:

$$R(T) = R_0 \ [1 + a \ T + b \ T^2 + c \ (T \quad 100\ C) \ T^3] \qquad (3.8)$$

With the coe cients: $a = 3;9 \ 10^{\ 3} \frac{1}{C}$, $b = \quad 5;8 \ 10^{\ 7} \frac{1}{C^2}$ and $c = \quad 4;2 \ 10^{\ 12} \frac{1}{C^4}$. The ouput of the sensor for $T = 0\ C$ is de ned as: $R_0 = R(T = 0\ C) = 100$.

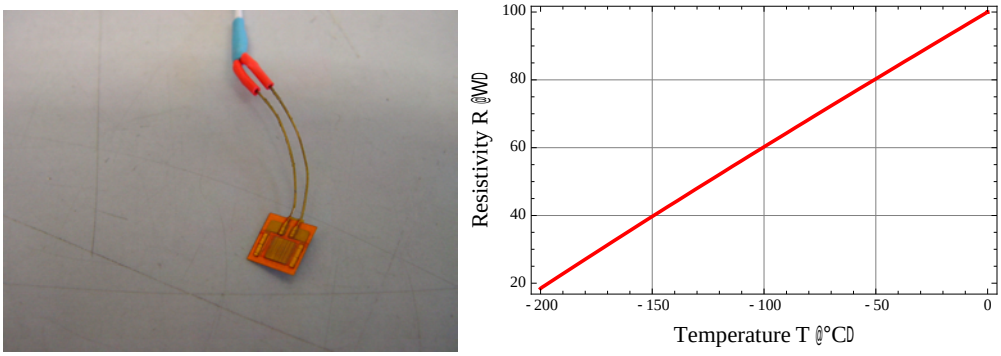

Figure 3.6: Left: Typical PT-100 sensor, used for the AGATA-detectors. Right: Plot of the PT100-resistivity $R(T)$ for low temperatures $T \quad 0\ C$.

The PT-100-sensors used for AGATA-detectors (gure 3.6 left) are xed at two positions: the rst is inside the cryostat on the copper rod of the dewar. The second PT100 is on the crystal-surface itself. Figure 3.7 shows the PT100-read-out of an cooling-in-process as the measured resistance has been translated into a temperature. For this reason equation 3.7 has been approximated by the following linear function:

$$R(T \quad 0\ C) \quad R_0 \ (1 + 4{:}02 \ \frac{10^{\ 3}}{C} \ T) \qquad (3.9)$$

The temperature decreases when liquid nitrogen is lled inside the dewar. After one hour the temperature has reached a minimum of $193\ C$. However the uctuations in the measured curve are caused by frequently lling of liquid nitrogen. During the cooling-in-process the dewar and its temperature are not in a steady state as the temperature is changing quickly with any amount of LN_2 lled in. The red curve in gure 3.7 is a t to the measured temperature $T(t)$ as a function of time:

$$T(t) = a \ \exp[\ b \ t] + c \qquad (3.10)$$

Fitting this equation to the measured data leads to the following coe cients: $a = (246 \quad 1)\ C$, $b = (3{:}80 \quad 0{:}04) \frac{1}{h}$ and $c = (\quad 194{:}2 \quad 0{:}3)\ C$. The uctuations are disregarded because they depend on the amount of liquid nitrogen lled in and are absolutely randomly. Except the uctuations the data is tted well by equation 3.8. Thus the temperature seems to decrease exponential during a cooling-in-process.

3.2.2 The Bias-shut-down

The critical temperature of the detector-system is about $T_C \quad 160\ C$, which is equivalent to a resistivity of $R(T_C) \quad 35$ on the crystal's surface.

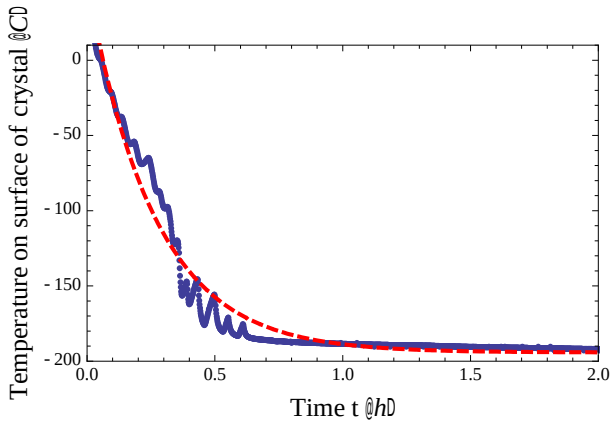

Figure 3.7: Temperature of the crystal's surface during a cooling-in-process. By using equation 3.8 the temperature has been calculated from the measured resistance of the PT100-sensor. The red curve is an exponential t to the measured temperature: $T(t) = a \quad e^{b} + c$ with coe cients a; b and c.

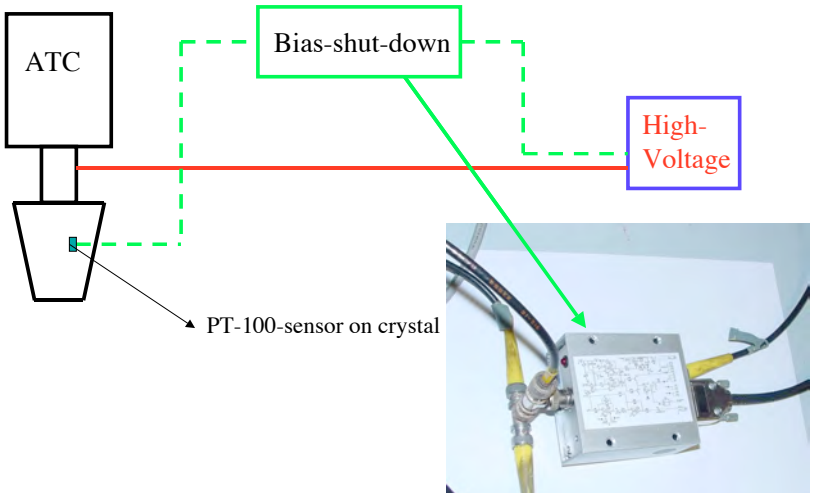

Figure 3.8: Schematic drawing and photograph of the bias-shut-down. The PT-100-signal is linked with the shut-down-system (right side on photograph), which is linked to the high-voltage power supply (left side on foto). For R ' 30 the shut-down-function is activated and ramps down the high-voltage immediately.

By reaching T_C the getter will start gasing out and the break-down voltage increases. Moreover the leakage current over the crystal's surface increases and may damage it. Thus the high voltage needs to be shut down, in order to protect the detector-electronics and the crystals. This can be achieved by a bias-shut-down, which is linked between the PT-100-sensor and the high-voltage-supply (g. 3.8). If the PT-100 has a resistance of R ' 30 (T 170 C), the bias-shut-down will ramp down the high-voltage.

The sensor is xed on the crystals surface and the crystal is linked through the cooling nger with the dewar. The cooling nger is made of copper, which has good thermal conduction. This means: If the dewar is getting warm and the getter starts gasing out already, the crystal will remain cold for a while due to its own and the cooling ngers' heat capacity. Hence the PT-100-sensor will not alarm the cryogenic lling system at the right time (before the getter starts gasing out). Therefore the only possibility for preventing damages of the detector-system is to release the bias shut down by the PT-100-sensor.

An other aspect of this monitoring-method is that the detector is not operational after a bias shut down since its temperature and the condition of its electronics need to be checked. The worst case is the separation of a detector unit from the array which is not trivial at all considering the few space between each detector (about 0.5 mm space between the endcap of each detector). Therefore a shut down of a detector unit causes an expenditure of time, a lack of the measurement period and extra costs. These problems can be overcome by a direct read out of the LN_2-level and provides an additional safety in operating such delicate detector systems.

3.3 The capacitive LN_2-read-out (I)

The LN_2- lling-level can be directly checked by measuring the capacity inside the dewar. For that reason a metallic cylinder has been mounted inside the inner dewar (red line in g.3.5 left). The dielectric constant of liquid nitrogen is $_{LN_2} = 1.4$ [APG] whereas the dielectric constant of nitrogen is 1. Thus a change in the lling level causes a change of the capacity C between the inner cylinder and inner dewar.

3.3.1 The steady state and vertical dewar-postion

Figure 3.9 shows a schematic drawing of a dewar in vertical position which is lled up to the height h with liquid nitrogen. Considering the gas phase of the nitrogen (indicated by N_2(g) and the liquid-phase (indicated by N_2(g)) being in thermal equilibrium a classical cylindrical capacitor may be used to describe the electrical properties of the dewar (see right hand side of g. 3.9). Using the equivalent circuit diagram (see g. 3.9) leads to the average dielectric constant $h_r i$ of the whole dewar:

$$h_r i = \frac{1}{h_0}\,[(h_0 \quad h) + {}_{r;l} \quad h]\,, \tag{3.11}$$

$$h_r i = \frac{1}{h_0}\,[h_0 + ({}_{r;l} \quad 1) \quad h]\,, \tag{3.12}$$

$$h_r i = 1 + 0.4\,\frac{h}{h_0} \tag{3.13}$$

As the dielectric constant for gasious nitrogen is equal to 1 and the dielectric constant for liquid nitrogen is 1.4 then the total capacity C of the dewar is given by:

$$C = 2 \quad {}_0 \quad \frac{h_0 \quad h_r i}{\ln \frac{r_2}{r_1}}\,) \tag{3.14}$$

$$\boxed{C(h) = \frac{2 \quad {}_0}{\ln \frac{r_2}{r_1}} \quad h_0 + 0.4h} \tag{3.15}$$

For the dewar in a vertical position the measuring capacity C is a linear function of the lling level h. Figure 3.10 shows a simulation of the lling capacity C(h) as a function of the lling level h when the liquid nitrogen level inside

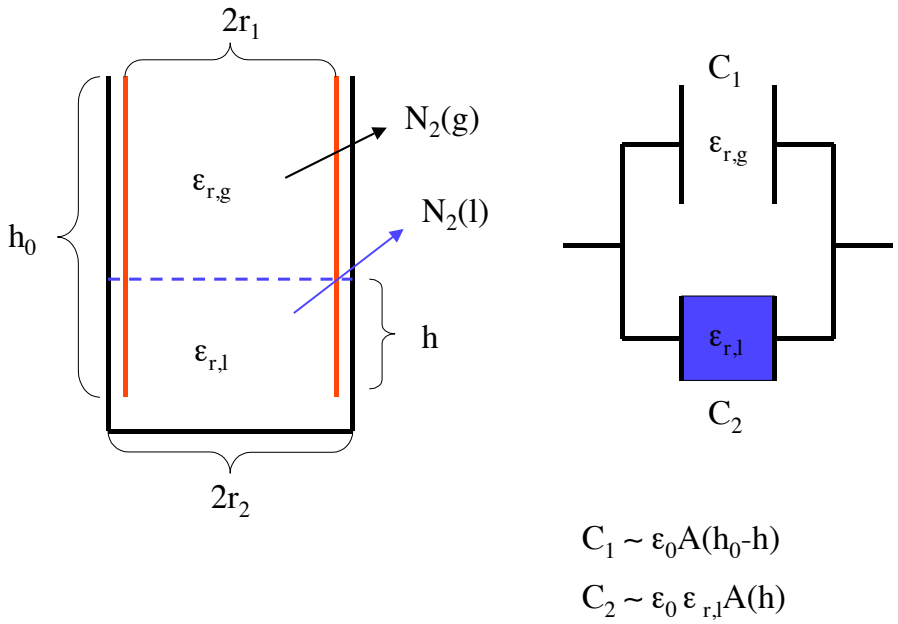

Figure 3.9: Left: Schematic representation of the dewar as a cylinder capacitor. The red line indicates the inner cylinder with radius r_1. The inner dewar's radius is r_2. The dewar has the total height h_0 and is lled up to h with liquid nitrogen. Because the system is in thermal equilibrium, this part can be represented by the dielectric constant $_{r;l}$ = 1:4 of LN_2. The upper part contains gasious nitrogen $N_2(g)$, which has the dielectric constant $_{r;g}$ = 1. Right: Equivalent circuit diagram of a dewar which is lled with LN_2. The capacity C_1 depends on $_0$ and the area $A(h_0 \quad h)$ whereas the capacity C_2 depends on the electrical constant $_{r;l}$ of liquid nitrogen and the area $A(h)$. Both capacities add up to the measured capacity $C = C_1 + C_2$.

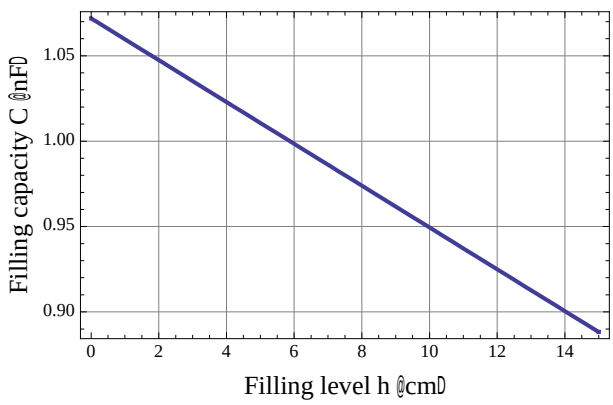

Figure 3.10: Simulation of the lling capacity C as a linear function of the lling level h. The simulation has been done for an ideal dewar with total height h_0 = 29 cm, radius r_2 = 10 cm and r_1 = 9:82 cm.

the dewar is decreasing. The expected values for the measuring capacities are a few nF. Considering this simulation, the variation between the maximum capacity $C(h = 0\,\text{cm})$ and the minimum capacity $C(h = 15\,\text{cm})$ varies about 21 % which is considerably low.

3.3.2 Measuring device (I)

The capacity inside a dewar is read out through a BNC-connector (gure 3.11 left), which has been connected to a multimeter. The rst capacitive measurements were done this way. Additionally, the multimeter has a digital output and is connected to a laptop (gure 3.11 right).

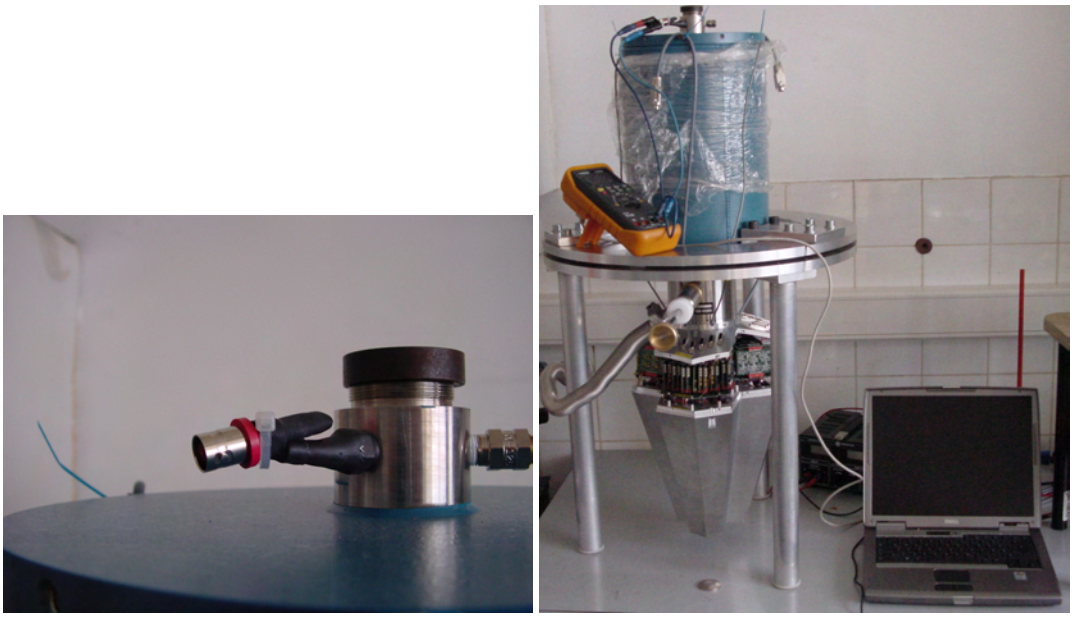

Figure 3.11: Left: BNC-connector for reading out the capacity. Right: Multimeter with digital-output, connected to a laptop.

First measurements and results

First of all, the capacity was measured with respect to the LN_2- lling level. This was done at ATC(1) (g. 3.12 a)) and repeated for ATC(3) (g. 3.12 b)) later. The capacity C was measured with a multimeter and the lling-level h was read out analogously. The red curves in g. 3.12 are linear regressions: $C(h) = m \quad h + C_0$. Using this and equation 3.12 leads to:

$$\frac{m}{b} = \frac{1}{h_0} [{}_{r;l} \quad 1] , \tag{3.16}$$

$${}_{r;l} = \frac{m}{C_0} h_0 + 1 \tag{3.17}$$

With $h_0 = (29 \quad 1)\,\text{cm}$, the value of ${}_{r;l}$ results in:

$$ATC(1) : {}_{r;l} = (1:29 \quad 0:02) \tag{3.18}$$

$$ATC(3) : {}_{r;l} = (1:31 \quad 0:01) \tag{3.19}$$

These values are not consistent with the true value of ${}_{r;l} = 1:4$. The measured capacity C depends strongly on the adjusted measuring-range of the multimeter. Thus the determination of ${}_{r;l}$ is less precise. Figure 3.13 represents the

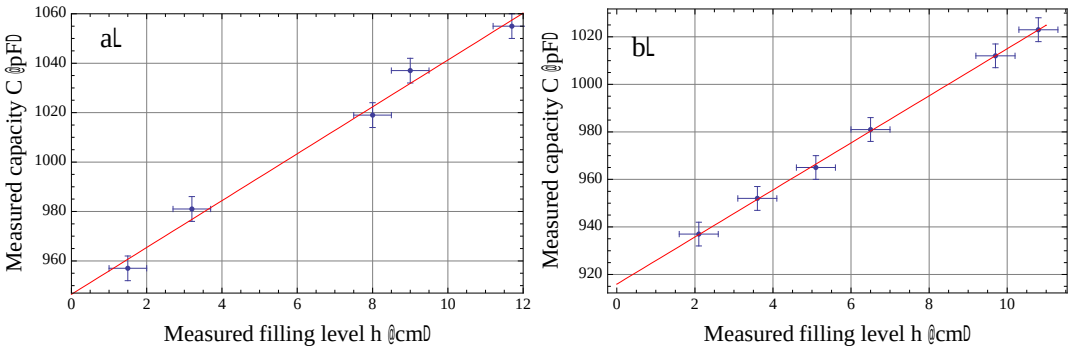

Figure 3.12: a) First capacitive read-out at ATC(1). The capacity C was measured with respect to the filling level h. The red curve is a linear regression $C(h)$ through the measured data: $C(h) = (9.48 \pm 0.59)\frac{pF}{cm} \cdot h + (947 \pm 5)\,pF$. b) The measurement was repeated for ATC(3) as the measured data was regressed by $C(h) = (9.91 \pm 0.11)\frac{pF}{cm} \cdot h + (916 \pm 1)\,pF$. The errors of the measured capacities are related to the multimeter and assumed as $\Delta C = 5\,pF$. The errors of the measured filling height h are assumed to be $\Delta h = 0.5\,cm$.

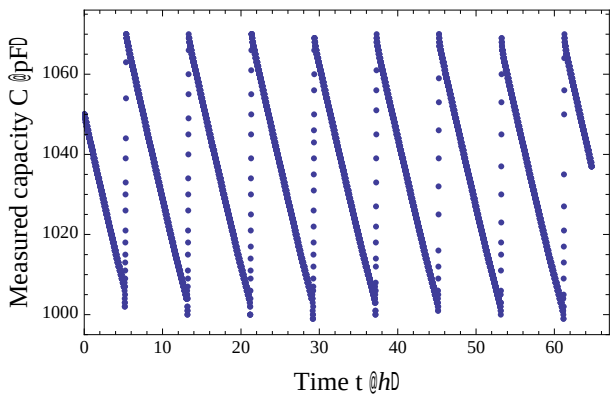

Figure 3.13: Over-weekend-measurement at ATC(2) during a filling-cycle. ATC(2) was connected to an automatic filling system, which refilled the detector with LN_2 every 8 hours.

results of an over-weekend-measurement of $C(h)$. It perfectly re ects the linear behaviour of $C(h)$, as C was measured with respect to the time and not to the lling height. The maximum capacity is C_{max} 1070 pF. The minimum capacity C_{min} of an empty dewar was not measured because the dewar has been re lled every 8 h. The lowest capacity which can be observed in g. 3.13 is C 1000 pF. The minimum capacity of a dewar C_{min} is referring to an empty where no liquid nitrogen is inside. But the dewar is still cold and the getter is not gasing out.

3.3.3 Cooling-in- and warming-up-process

Considering a cooling-in or warming-up-process, the liquid phase $N_2(l)$ and the gas phase $N_2(g)$ are not in thermal equilibrium and therefore equation 3.14 is not valid anymore. The mean dielectric constant of the dewar is now strongly time-dependent. Figure 3.14 (left) shows that the liquid nitrogen is boiling

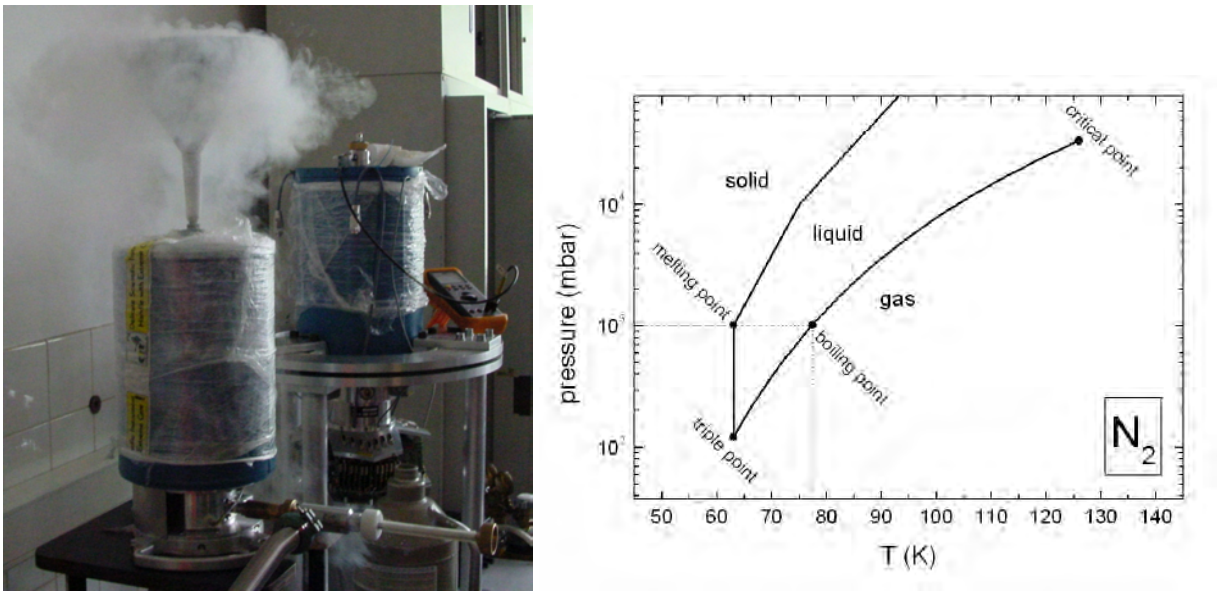

Figure 3.14: Left: Cooling in of an AGATA-single-cryostat. The LN_2 is boiling at room temperature. Right: Phase diagram of liquid nitrogen [Thr08].

under pressure and steam development while a cryostat is cooled in. The right hand side of g. 3.14 displays the phase diagram of liquid nitrogen. Since the liquid nitrogen is lled into the dewar at room temperature and normal pressure, the phase of the LN_2 is far away from the critical point. Thus the liquid phase and the gas phase of nitrogen are co-existing.

Cooling in an AGATA-triple-cryostat

The data during a cooling-in-process are shown in gure 3.15 where two structures are striking: the rst one is visible in diagram a) of g. 3.15. The second one is a minimum of the measured capacity at 15 min. The expansion of this diagram (see g. 3.15 b)) points out several peaks which have already appeared in g. 3.7. When liquid nitrogen is lled into the dewar for the rst time, the whole material is working under thermal contraction. As the temperature of the whole system is not constant, the dewar is getting warm immediately, as long as no LN_2 is lled in. The material starts to expand.

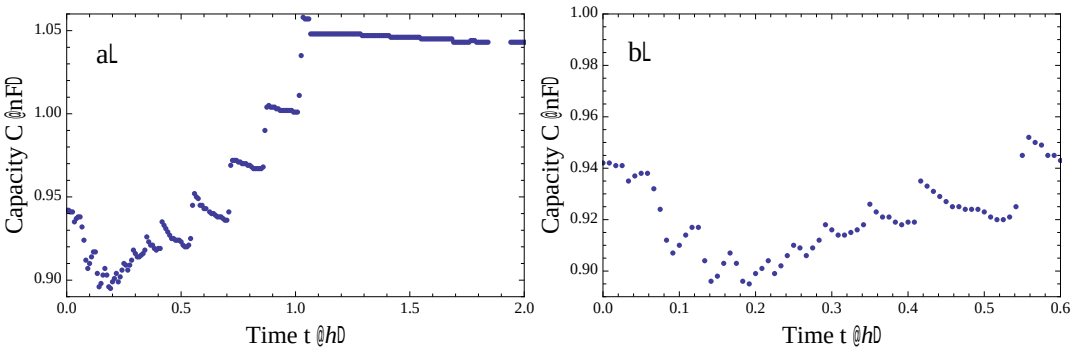

Figure 3.15: a) Cooling-in-Process of an AGATA-triple-cryostat. b) Expansion of the left gure. The measured capacity C decreases in the rst 15 min but increases after that point. The thermal equilibrium is reached approximately after one hour, because C(t) is linear as a function of time.

When LN_2 is lled in again the temperature decreases rapidly and the dewar-material is contracting. This process, namely the expansion and contraction of

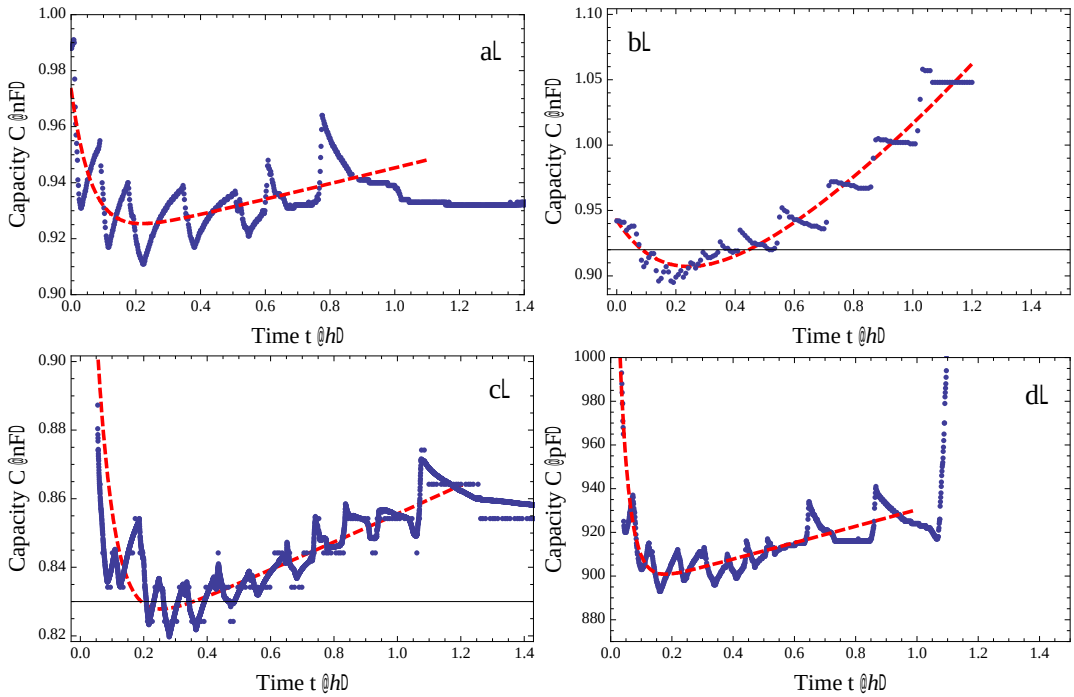

Figure 3.16: Comparison of the function $C_R(t)$ (red curve) within the measured data during several cooling-in-processes. a) Cooling-in-process of ATC(2). b) Cooling-in-process of ATC(4). c) and d) Cooling-in-process of ATC(3).

the dewar (including the rest of the cryostat), will repeat itself until the temperature of the system is in equilibrium. The liquid nitrogen inside the dewar strongly boils until the cryostat is cooled down to 190 C and the lling level and the dielectric constant behave in an irregular way. These considerations may be reasonable for the peaks of the measured capacity which are displayed in diagram b). Moreover the height and width of each peak depends strongly on the amount of liquid nitrogen lled in during a cooling-in-process. Taking a closer look at diagram a) again points out that the measured capacity decreases in the rst 15 min of the cooling-in-process. After that the capacity increases as a function of the lling height. Figure 3.16 shows the measured

data during four-cooling-in-processes. The red curve in each diagram is a t $C_R(t)$ to the measured data which only considers the thermal contracting of the dewar. Diagram a) of g 3.17 shows the variation of the factor $\ln\frac{r_2}{r_1}^{1}$ as a function of the distance $r = r_2 \quad r_2$, as r_1 is the radius of the inner cylinder and r_2 the radius of the inner dewar respectively. The distance r between the inner cylinder and inner dewar is 5 mm when the cryostat is at room temperature. Diagram a) points out that even small variations of r lead to considerable high variations of the factor $\ln\frac{r_2}{r_1}^{1}$ which a ects the measuring capacity C (see equation 3.14). Due to the thermal contraction of the dewar during a cooling-in-process the radius r_2 and r_1 depend on the temperature T of the system:

$$\ln\frac{r_2}{r_1} = \ln\frac{r_2(T)}{r_1(T)} \tag{3.20}$$

The temperature dependence of a solid with length l is given by [Dem04]:

$$l(\quad T) = l_0 \ (1 + \qquad T) \tag{3.21}$$

l_0 is the length at room-temperature and T the change in temperature. The coe cient is called the **coefficient of expansion** and is material speci c constant. Considering the temperature-measurement discussed in section 3.2.1 it is shown that the temperature decreases exponentially:

$$T(t) = a \ e^{bt} + c \tag{3.22}$$

Assuming that the derivative $\frac{dT}{dt}$ can be approximated by $\frac{T}{t}$ and that t is a constant time interval (e.g. the measuring time) leads to:

$$T = \quad e^{bt} \tag{3.23}$$

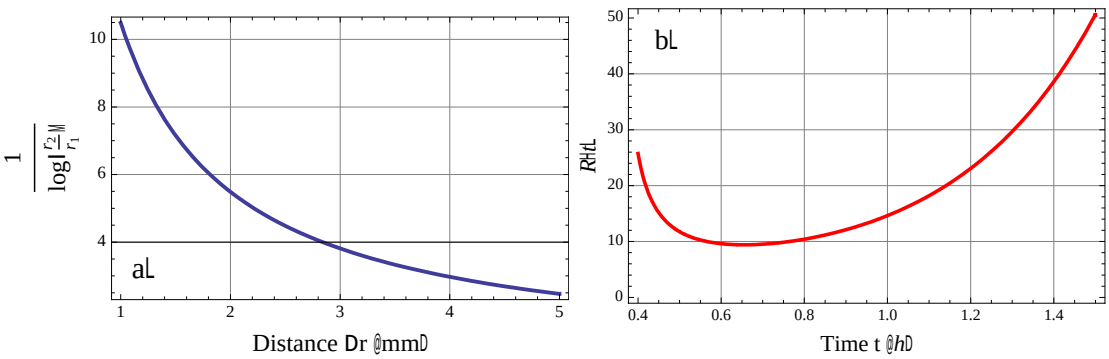

Figure 3.17: a) Variation of $\ln\frac{r_2}{r_1}^{1}$ as a function of the distance $r = r_2 \quad r_1$ between the inner cylinder and the inner dewar. b) Plot of the contraction function $R(t)$ as a function of time with arbitrary parameters: $\frac{r_{0;2}}{r_{0;1}} = 1$, $c_2 = 2$, $b_2 = 3$, $c_1 = 4$ and $b_1 = 5$.

Using this for equation 3.20 results in:

$$r(t)_i = r_{0;i} \left[1 + c_i \ e^{b_i t}\right]^{i} ; \ c_i = \qquad {}_i ; \ i = 1;2 \tag{3.24}$$

$r_{0;2}$ is the radius for the inner dewar in case of constant temperature and $r_{0;1}$ the radius for the inner cylinder respectively. Considering the thermal coupling, thickness and xing inside the dewar, the inner cylinder and inner dewar should behave slightly di erent during a cooling-in-process and therefore the coe cients b_i and c_i are for each radius di erent. This leads to the following function:

$$R(t) := \ln \frac{r_{0;2}}{r_{0;1}} \frac{(1 + c_2 e^{b_2 t})}{(1 + c_1 e^{b_1 t})} \qquad (3.25)$$

R(t) shall be called the **contraction function**. A plot of R(t) as a function of time is shown in diagram b) of gure 3.17. Comparing this simulation and the capacity measurement shown in gure 3.15 point out a similar structure. For a rst consideration of the capacity C during the cooling-in-process, the average dielectric constant $\langle \varepsilon_r \rangle$ inside the dewar has been approximated as: $\langle \varepsilon_r \rangle \quad 1$. Thus the capacity C during a cooling-in-process is approximated by the capacity C_R:

$$\boxed{C(t) \quad C_R(t) = 2 \quad {}_0 h_0 \quad R(t)} \qquad (3.26)$$

The ts of $C_R(t)$ to the measured data is not very accurate for the cooling-in-process of ATC(2) (see g. 3.16), whereas the measured capacity C of ATC(3) and ATC(4) is approximated very well by $C_R(t)$. Thus the decrease of the measured capacity during the rst 15 min of a cooling-in-process and the increasing of C after that time are related to the thermal contraction of the dewar.

Describing the peaks of C is not trivial because they depend on the amount

Cryostat	c_1	c_2	b_1 [1=h]	b_2 [1=h]
ATC(2)	17:11 0:79	16:03 0:74	15:98 1:35	15:98 1:35
ATC(4)	7:93 0:54	7:38 0:51	4:78 0:63	4:79 0:63
ATC(3), c)	3:66 0:03	3:4 0:03	18:52 0:25	15:98 1:35
ATC(3), d)	0:0695 0:0001	0:0177 0:0002	0:042 0:002	29:4 0:7

Table 3.1: Fit-paramters $c_1; c_2; b_1$ and b_2 of the function $C_R(t)$ which is shown in g. 3.16. The ratio $\frac{r_{0;2}}{r_{0;1}}$ has been set as 1.

of liquid nitrogen which is lled into the dewar. Table 3.1 shows the t-parameters of $C_R(t)$. The coe cient pairs $c_1; c_2$ and $b_1; b_2$ for one cryostat do not di er very much from each other. This is not surprising, since the inner cylinder and inner dewar are made of the same material and e ects like thermal coupling should not have any signi cant e ect. Comparing the coe cients of

the third and fourth row of table 3.1, shows a discrepancy while the cryostat is the same.This discrepancy between the coe cients is related to the experimental conditions, like the amount of LN_2 lled in, which were not accounted for. The experimental conditions are also reasonable for the complexity of an exact t of C(t) during a cooling-in-process.

Warming-up-process

The warming-up-process is another process in which the thermal equilibrium is not valid after a certain time. In principle R(t) with di erent parameters is applicable to describe C(t) during this process but this will not be treated in this section. One important aspect of measuring C(t) during a warming-up-process is the determination of C_{min} and C_{max}. C_{min} is the capacity of the dewar when no liquid nitrogen is inside, but the dewar is still cold and the getter does not start gasing out. C_{max} is the capacity in case of a completely

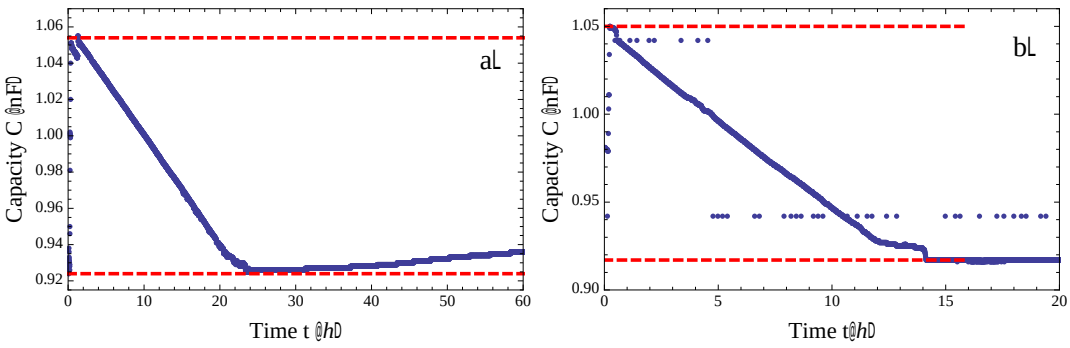

Figure 3.18: a) Warming-up-process of ATC(4). b) Warming-up-process of ATC(3). The red dashed lines indicate C_{min} and C_{max}.

lled dewar. The capacity C(t) was measured as a function of time during two warming-up-processes for two di erent triple clusters. The results of these measurements are displayed in g. 3.18. The measurements were done with ATC(4) and ATC(3) (further warming-up-processes are shown in appendix A). The red lines in both diagrams indicate the minimum capacity C_{min} and the maximum capacity C_{max}. The measured values are listed in table 3.2. The

Cryostat	C_{min} [pF]	C_{max} [pF]	$C = C_{max} \quad C_{min}$ [%]
ATC(4)	924 5	1054 5	12.3 0.6
ATC(3)	917 5	1050 5	12.7 0.6

Table 3.2: Measured minimum capacity C_{min} and maximum capacity C_{max} for ATC(3) and ATC(4). The di erence capacity $C = C_{max} \quad C_{min}$ is evaluated in %.

di erence between a full and empty dewar is about 14%. The left diagram in g. 3.18 also reveals a behaviour of C(t) opposite to the cooling in process. At rst, C(t) decreases nearly linearly (see equation 3.15). When the

LN_2-reservoir is exhausted, the non-equilibrium-environment starts and the contraction function is not constant anymore. Thus the inner cylinder and inner dewar start to expand slowly and the capacity increases over a long time period until the whole dewar is at room temperature. The measurement with ATC(4) was stopped after 60 hours, whereas the warming-up-process itself was not completed at that time.

Another interesting aspect is the consumption of liquid nitrogen, which is slightly di erent for each cryostat and depends on whether the cryostat is fully equipped with detectors, the preampli er stage is under operation and whether high voltage is applied. By looking again at g. 3.18, a considerable di erence between the LN_2-consumption of the two cryostats is visible. ATC(4) (see g. 3.18 left) is not equipped with electronics and detectors, whereas ATC(3) is fully equipped (but not biased). However the empty cryostat of ATC(4) lasts 22 h; a huge di erence of 8 h compared to the LN_2-consumption of ATC(3).

Chapter 4

LN_2-consumption-measurements

The LN_2-consumption is the important feature for operating the AGATA detector-cryostat. Consumption-measurements were performed with the following three AGATA triple clusters: ATC(2), ATC(3) and ATC(4). All capacitive measurements were performed with measuring device (I) which has been discussed in chapter 3.

4.1 LN_2-consumption of ATC(2)

The consumption-measurement performed with ATC(2) shows how the consumption is in uenced by applying high / low voltage and the room temperature. Furthermore, the direct read out by measuring the LN_2 lling height and the capacitive read out shall be compared.

4.1.1 Setting up ATC(2)

The consumption-measurements of ATC(2) were done over four days. The dewar was lled manually each day and the measurement started 30 min after that, so there was enough time for the lled in LN_2 inside the dewar to settle down.The capacity and LN_2- lling-height have been checked every hour. The LN_2-consumption of ATC(2) has been measured under three di erent conditions:

ATC(2) being operated with high and low voltage

ATC(2) being operated without any voltage

ATC(2) being operated with low voltage and high voltage which was ramped up slowly. Moreover, the XIA-electronics was running[1]

In order to provide equal conditions for each measurement, the pressure inside the dewar and the amount of liquid nitrogen at the beginning of each measurement were kept constant. Figure 4.1 shows several closings for the AGATA-dewar. ATC(2) was closed with a lead piece with a hole in the middle (closing d)) which has the advantage that the pressure inside the dewar is always in balance with the pressure of the environment. The lead piece has also no valve which might freeze up (like closing d) in g. 4.1) and cause a built up pressure inside the dewar. Since the pressure inside the dewar is still

[1] If the XIA-electronics is running the room temperature increases apreciably which might in uence the consumption.

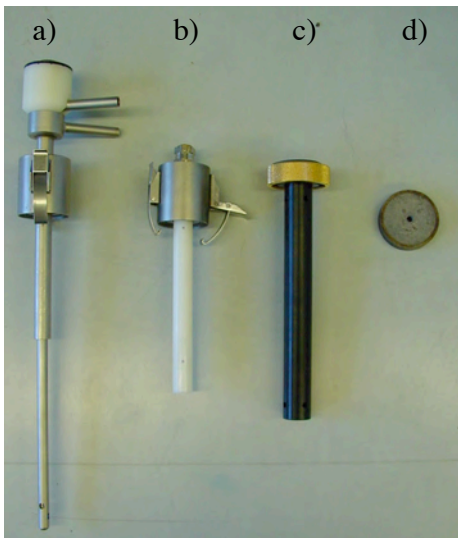

Figure 4.1: Four di erent closings for an AGATA-triple-cryostat. a) lling nozzle for connecting the detector to the automatic lling system. b) dewar closing with valve (on top) which opens at an internal pressure of one bar.c) dewar closing without any valve. d) lead piece with a 2 mm hole in the middle to avoid build up pressure.

high after a rst lling, a re-opening would cause a burst of liquid nitrogen and therefore the lling height $h(t = 0h)$ could not be determined.

4.1.2 Results: ATC(2)

The results of the capacity measurements under di erent conditions are displayed in g. 4.2. Diagram a) shows a plot of the measured capacities related to time, where all curves show a linear dependency between the measuring capacity C and the time t. The blue (high and low voltage) and black curve (low and high voltage and xia-electronics running) have the same gradient but di erent axis-intercept which is related to (slightly) di erent lling heights at the beginning of each measurement. The green curve (no high and low voltage) has a di erent slope than the others which indicates a lower LN_2-consumption. Diagram b) displays the same data, as the blue curve has been shifted by the di erence C between the maximum capacity $C(t = 0)$ of the black and blue curve. This diagram points out that there is no severe di erence between the slopes of the blue and black curve. Thus **the LN_2-consumption predominantly depends on the applied low voltage**. Diagram c) and d) show the measured lling height h which has been measured with respect to the time t (The measured lling heights are displayed in appendix B.). The measured capacity and the lling-height are strictly linear in time and thus can be described by:

$$C(t) = m_C \; t + b_C \tag{4.1}$$

$$h(t) = m_h \; t + b_h \tag{4.2}$$

m_C, b_C, m_h and b_h are t-parameters. A t of equation 4.2 to the measured lling heights is shown by the red curve in diagram c) and d) and therefore

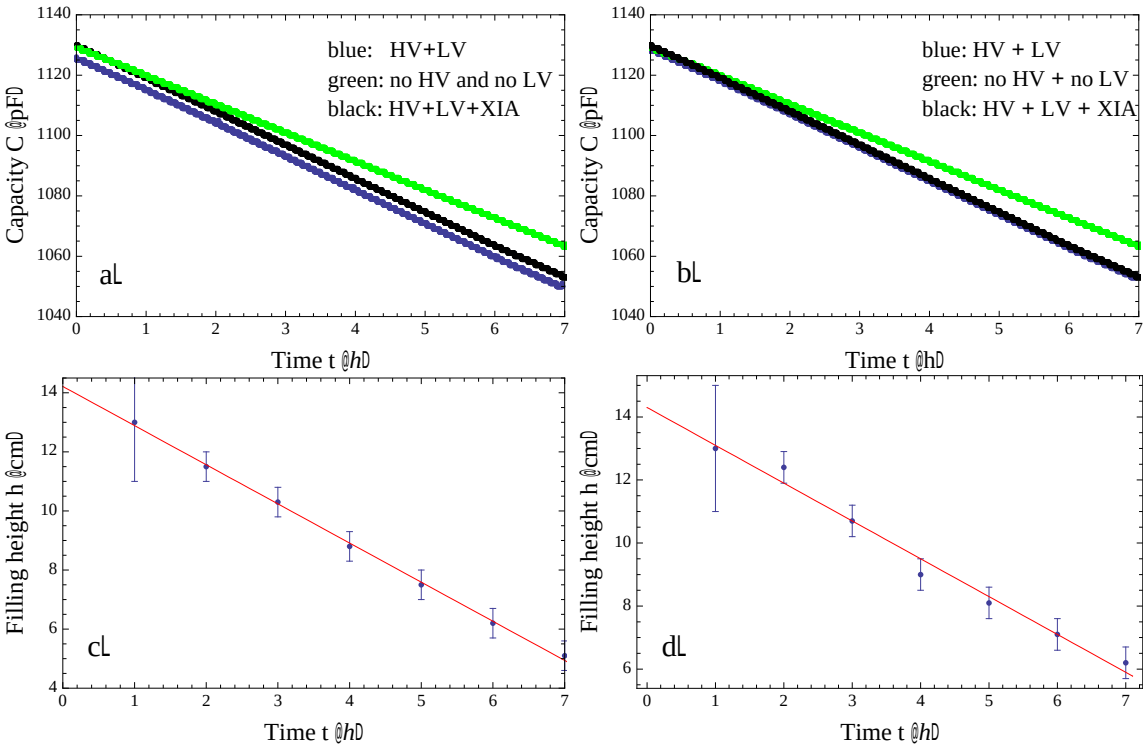

Figure 4.2: a) Measured LN_2-consumption for ATC(2) under di erent conditions (HV = high voltage, LV = low voltage). b) The blue curve has been shifted by the constant value $C = 3\,pF$ which compensates the indi erent lling height at the beginning of each measurement. Thus they are overlapping now. c) Measured LN_2- lling-level for ATC(2) which has been operated with high and low voltage. The red curve is a linear regression $h(t) = (1.33 \pm 0.02)\frac{cm}{h}\, t + (14.2 \pm 0.1)\,cm$. d) Measured LN_2- lling-level for ATC(2) without any voltage applied. The function of the tted curve here is given by: $h(t) = (1.2 \pm 0.07)\frac{cm}{h}\, t + (14.3 \pm 0.1)\,cm$.

the LN_2-consumption and operation time are given by:

$$= \frac{m_h}{b_h} \quad 4{:}5\,l \tag{4.3}$$

$$h(\ ) = 0 \ , \qquad = \frac{b_h}{m_h} \tag{4.4}$$

The factor 4:5 l is equal to the maximum amount of liquid nitrogen which can be hosted inside the dewar being in vertical position. The operation time of a detector depends on the di erent system-conditions, before the liquid nitrogen reservoir is completely consumed. Table 4.1 summarises the measured

Low voltage	h i $\frac{ml}{h}$		$_W$ [W]		[h]	
ON	419	19	18:65	0:85	11	0:5
OFF	378	23	16:83	1:02	12	0:7

Table 4.1: Summary of the consumption measurements at ATC(2). is the operation time of the detector-system under two di erent conditions: low voltage on or o .

consumption of liquid nitrogen and operation time. The operation time varies up to one our between operating the system with low voltage turned on or o . The evaporation heat Q_V and density $_{LN_2}$ of liquid nitrogen are: Q_V = 198:6$\frac{kJ}{kg}$ and $_{LN_2}$ = 0:807$\frac{kg}{l}$. Thus the LN_2-consumption $_W$ expressed in Watt is given by: $_W$ = Q_V . The values for $_W$ are also listed in table 4.1. Considering them, the applied low voltage is equivalent to an extra heat loss about 2 W which is related to the heat loss of the FETs (20 mW per channel, as each triple-cluster consists of 111 channels) in the cold part [JE08].

4.2 LN_2-consumption of ATC(3): The capton-cable-test

Two di erent sets of cables inside the cold part of ATC(3) have been tested for this consumption-measurement. The FETs in the cold part are linked through a cable harness with the feedthroughs to the warm part. The rst set of cabling is used in all AGATA-triple-clusters and single cryostats so far. The characteristics of these cables are a low thermal conductivity but a rather high electrical conductivity. The second set of cabling consists of copper wires which are coated with capton (seef ig. 4.3). This new

Figure 4.3: Second set of cable harness: copper wires which are coated with capton.

cabling is considered to be more robust and reproduceable in production, in comparison to the old cabling. To see the di erent in uence of the old or new cabling, the following issue has to be considered, namely: how does the new cabling in uence the cooling of the detectors and their LN_2-consumption. The results related to this issue are described in the following section.

4.2.1 Setting up ATC(3)

The setup of ATC(3) was similar to the one of ATC(2), whereas a dewar closing with valve (see g. 4.1) was used instead of a lead piece. ATC(3) was operated with preampli er-voltage on. The rst consumption-measurement has been performed with the old cabling for all three crystals, whereas the second measurement was done with the capton-cabling for all three crystals.

4.2.2 Results: ATC(3)

The results of both capacitive measurements are displayed in diagram a) of g. 4.4. Both curves have a di erent maximum capacity $C(t = 0)$ which is related to a di erent lling height at the beginning of each measurement. For that reason the orange curve has been shifted by $C = 14$ pF with respect to the y-axis (see diagram b) in g. 4.4). Both curves have a di erent gradient, caused by a higher LN_2-consumption of the capton cable harness. The measured data

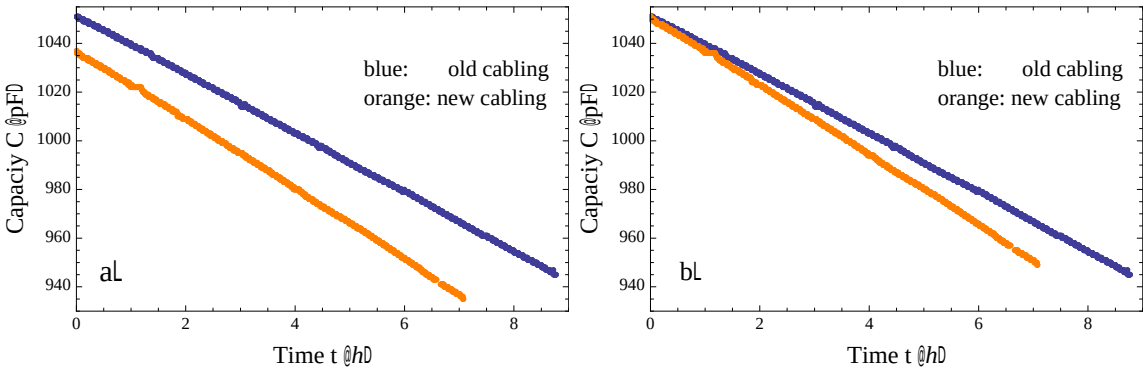

Figure 4.4: Measured LN_2-consumption for ATC(3). a) Measured capacity C for the new and old cabling. b) The orange curve is shifted by $C = 14$ pF with respect to the y-axis.

is tted equation 4.1[2] and therefore the consumption is given by:

$$= m_C \quad \frac{4:5\,l}{C} \tag{4.5}$$

C is the di erence between the maximum and minimum capacity of the dewar. This was already determined in chapter 3 to be: $C = (133 \quad 5)$ pF. The operation time can be determined by using:

$$= \frac{4:5\,l}{} = \frac{C}{m_C} \tag{4.6}$$

[2]The measured lling heights and a linear regression of them are shown in appendix B

Cabling	$_C$ [ml=h]	$_W$ [W]	[h]
old cabling	414 16	18:43 0:71	10:9 0:4
Capton	489 19	21:77 0:85	9:2 0:4

Table 4.2: Consumption value , $_W$ and operation time for the two di erent cabling-setups.

Table 4.2 shows the measured consumption values for the two di erent cabling-sets. The measured operation time for ATC(3) being equipped with the old cabling is consistent with the measured operation time of ATC(2) being operated with low voltage. Considering the 2 W heat loss due to operating the FETs, points out that the capton cabling causes an extra heat loss of 3:34 W.

4.2.3 Vacuum-leak in ATC(3)

Further tests with ATC(3) being equipped with the capton-cabeling inside could not be done because the detector got warm. Fortunately the LN_2-consumption was measured before the warm up, as the detector was linked to the lling system and a lling period of 8 hours was used. Diagram a) of gure 4.5 shows the measured capacity $C(t)$ as a function of time. The slope of each curve is changing by time which is only reasonable for an indi erent consumption of liquid nitrogen.

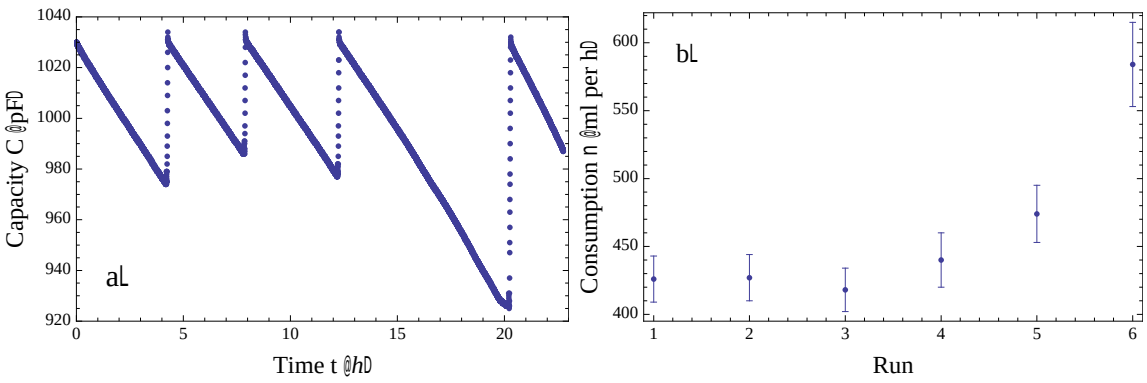

Figure 4.5: a) Measurement of the capacity C of ATC(3) equipped with capton-cabeling. The slopes of the curves di er as a function of time, indicating a change in the LN_2-consumption.

Each slope has been tted by equation 4.1 and the consumption was calculated by using equation 4.5. The results of this procedure are displayed in diagram b) of g. 4.5, where is plotted with respect to each measuring run. The consumption varies slightly around $425\frac{ml}{h}$ during the rst three runs, but increases after the third run up to $585\frac{ml}{h}$. Thus an instability of the consumption appeared during the measurement which caused a variation of about 38 %.

What happened?

An increased consumption value is in most cases related to a thermal contact between endcap and the interior of the detector or to a vacuum leak, such as a broken feedthrough, which actually happened to ATC(3). As a consequence the pressure inside the cryostat and the consumption of LN_2 increased. Furthermore, the outer endcap was cooled and its temperature fell below the dew point and therefore the whole detector got wet at the surface (see g. 4.6). The pressure inside the cryostat increased due to the broken feedthrough from

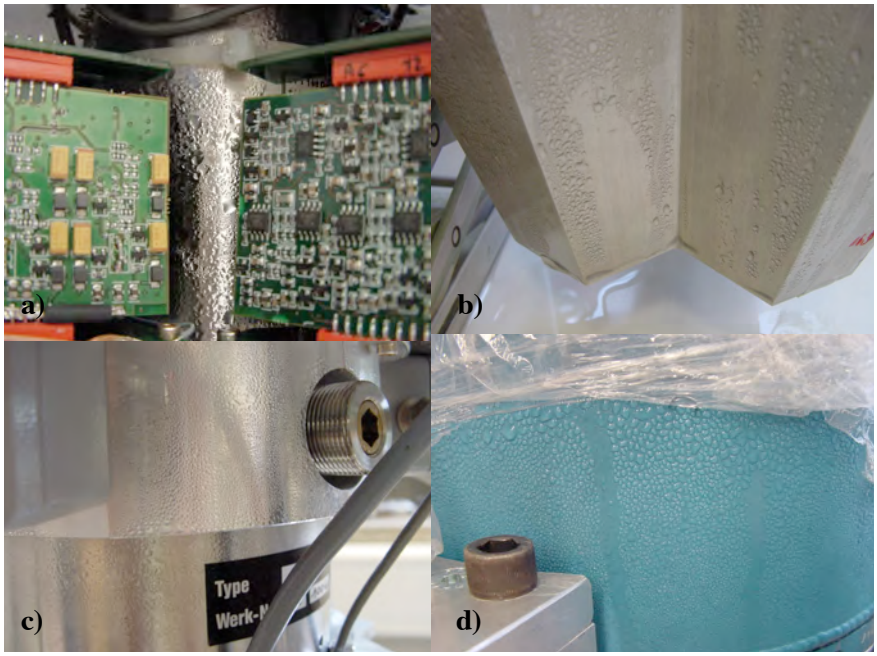

Figure 4.6: Status of ATC(3) after the vacuum broke. a) Flange near the warm preampli er is covered with water. b) The endcap is totally wet. A temperature of 12 C (which is below the dew point) has been measured in some regions. c) The ange near the high voltage feedthrough got also wet. d) The dewar was covered with water and had a temperature of 14 C.

10^{-7} mbar to 10^{-4} mbar. As a consequence, the cabling has been changed back to the old cabling and the broken feedthroughs were repaired.

4.3 LN_2-consumption of ATC(4)

Considering the results gained in the previous sections, the question arose, how the consumption of the cryostats reacts to di erent loads (e.g. low voltage, di erent cabeling, change in electronics). The change in the LN_2-volume is given by:

$$V(t) = \quad t + V_0 \tag{4.7}$$

t is the amount of liquid nitrogen which is needed to keep the detector at a certain temperature at the time t. Figure 4.7 shows the schematic drawing of an AGATA-cryostat which is treated as ideal for simplicity. A heat loss through the copper-rod or thermal coupling with the environment are neglected. The crystal with temperature T_1 is linked by the copper-rod with the LN_2-reservoir with temperature T_2. The system reaches a steady state after a certain time, so

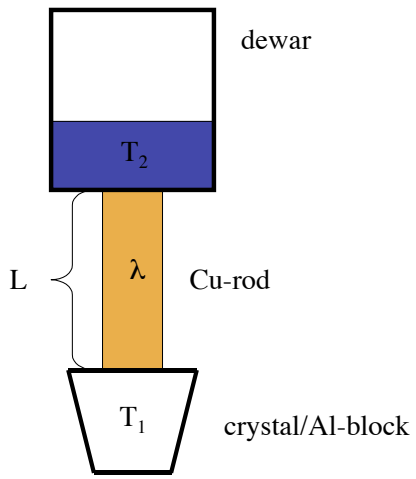

Figure 4.7: Schematic drawing of an AGATA-cryostat. The dewar is linked by a copper-rod (cooling nger) with the Ge-crystal, or Aluminium-block in the case of ATC(4). The dewar with liquid nitrogen inside has the temperature T_2, whereas the crystal/Al-block has the temperature $T_1 > T_2$. The copper-rod has the length L and thermal conductivity .

that a constant amount of heat is oating through the rod from the crystal to the dewar [Dem04]. Despite the temperature di erence $T_1 \quad T_2$, this heat ow depends on the length L, the sectional area A and the thermal conductivity of the copper rod [Dem04]:

$$\frac{dQ}{dt} = (T_1 \quad T_2) \quad \frac{A}{L} \tag{4.8}$$

As the LN_2-reservoir is constantly heated by $\frac{dQ}{dt}$, the consumed amount of liquid nitrogen per time is given by:

$$Q_V \quad {}_{LN_2} = \frac{dQ}{dt}, \quad = (T_1 \quad T_2) \quad \frac{A}{Q_V L \quad {}_{LN_2}} \tag{4.9}$$

As ${}_{LN_2}$ is the density, Q_V the evaporation heat and the consumption of liquid nitrogen. In this simpli ed model the consumption of liquid nitrogen depends on the temperature T_1 of the crystals and the characteristics of the cooling nger. Since $\frac{dQ}{dt}$ is constant, the amount of heat P_{in} which is induced into the cooling nger is equal to equation 4.8. Thus the consumption of liquid nitrogen is given by:

$$\boxed{= \frac{1}{Q_V} \quad P_{in}} \tag{4.10}$$

4.3.1 Setting up ATC(4)

For the purposes mentioned above, the cryostat of ATC(4) (picture a) g. 4.8) has been equipped with three aluminium blocks (picture b) g. 4.8) and a caddock (picture c) g. 4.8). In principal a caddock is a resistor which creates heat when voltage is applied. A caddock is used for annealing a cryostat which needs to be done when the getter is saturated after several cooling-in-processes or a long operation-time. The getter is heated by the caddock and starts gasing

out. Hence the cryostat has to be pumped in order to get the gas molecules out of the system. If P is the heating power of the caddock, the injected heat per time yields for:

$$P_{in} = \quad (P + P_0) \tag{4.11}$$

The factor determines how much heat radiation produced by the caddock is injected into the cooling- nger and heats the LN_2-reservoir. depends on the heat-conductivity of the copper rod and the surrounding material, such as the aluminium blocks, the attachment for the crystals etc. P_0 is the amount of heat which is frequently emitted by the material attached at the cooling nger. Thus the liquid nitrogen consumption as a function of the applied heating power is given by:

$$(P) = m \quad P + \quad _0 \tag{4.12}$$

As $m = \frac{}{Q_V}$ and $_0 = \frac{P_0}{Q_V}$. The caddock has been xed directly on the cooling nger (picture d) g. 4.8) in order to measure the in uence of the applied heating power on the consumption. Apart from the aluminium blocks

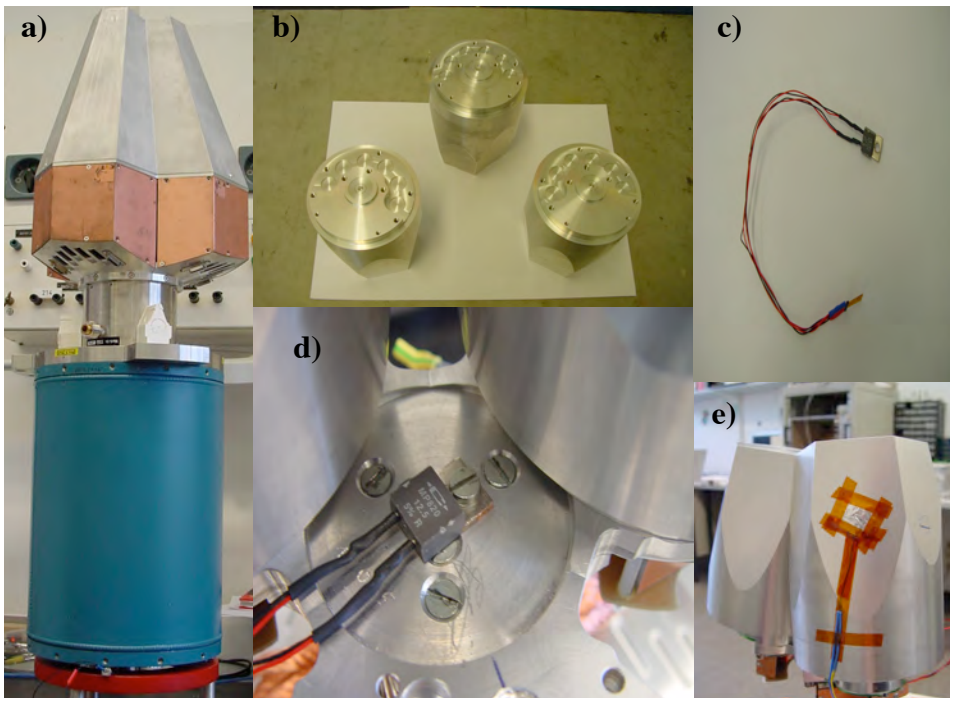

Figure 4.8: a) The cryostat of ATC(4), equipped with no crystals and no electronics inside. b) Three asymmetrical aluminium blocks of A, B and C-type. Each block has a mass of $m_{block} = 1:6$ kg. c) Caddock with a resistance of $R = 13$. d) The caddock been mounted directly onto the cooling nger and between the aluminium blocks. e) In order to check the temperature a PT100-sensor has been xed on the outside of a block.

and the caddock a PT100-sensor has also been xed on one block (picture e) g. 4.8) so that the temperature inside the cryostat could be checked. Again the capacity has been read out with measuring device I. The caddock was biased with a standart power supply unit, which can be seen in g. 4.9.

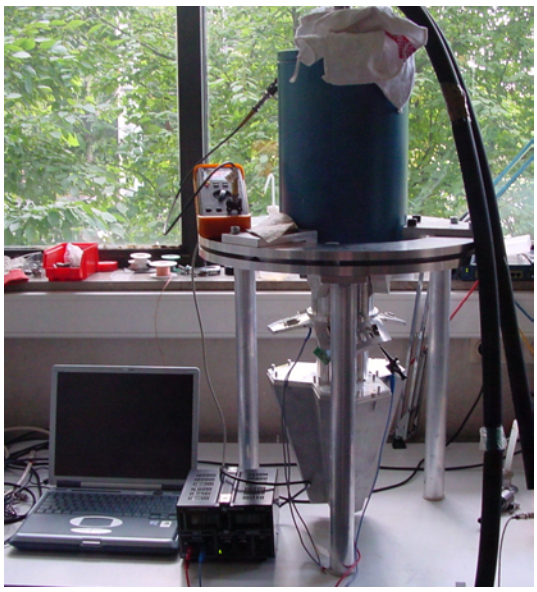

Figure 4.9: The cryostat of ATC(4) is equipped with aluminium blocks inside and plugged to the automatic lling system. The caddock is linked to an external power supply unit (black box) and the capacity is read out by using measuring device I.

4.3.2 Cooling-in ATC(4)

After preparing the system for the consumption-measurement, the cryostat was cooled in and directly linked to the automatic lling system. The consumption was measured over two lling periods. Figure 4.10 shows the results of this measurement. Diagram a) displays the measured capacity as a function of time. The slope of $C(t)$ is changing by time which indicates a change of the consumption . Diagram b) of g. 4.10 displays the measured consump-

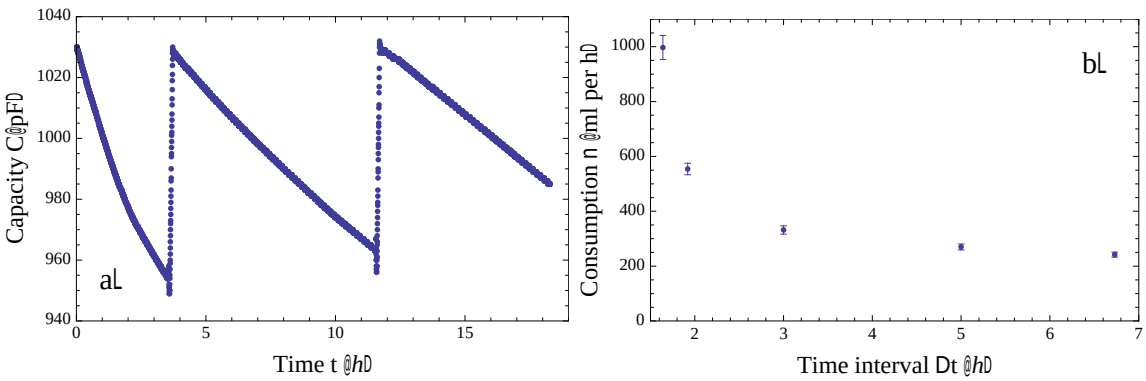

Figure 4.10: a) Measured capacity $C(t)$ as a function of time during one lling cycle. The curves are changing within one period of 8 hours. b) Measured LN_2-consumption after cooling in ATC(4) as a function of the time intervals in which the consumption did not change.

tion of liquid nitrogen as a function of time. According to equation 4.9 the consumption of liquid nitrogen is direct proportional to the di erence $T_1 - T_2$ between the temperature T_2 inside the dewar and the temperature T_1 of the whole material which is attached at the cooling nger. The temperature T_2 is constant, whereas T_1 is changing by time after cooling in. Thus the consumption changes as long as T_1 is not constant. Considering a one dimensional

heat ow inside the copper rod, the change of T_1 as a function of time is given by [Dem04]:

$$\frac{@T_1}{@t} = \frac{}{c \quad _{rod}} \frac{@^2T_1}{@x^2} \tag{4.13}$$

is the heat conductivity, $_{rod}$ the density and c the heat capacity of the copper rod. Thus the temperature T_1 changes as longs as the temperature gradient inside the cooling nger is not constant. The condition $\frac{@T_1}{@t} = 0$ (steady state) is prerequisite for equation 4.8.

4.3.3 Results of the consumption tests

The capacity has been measured during one lling-cycle (see section 4.3.1) and each measurement lasted 22 h. The heating power was changed for each measurement by biasing the caddock with di erent voltages. One run is shown in g. 4.11 where the heating power is $P = 2\,W$. Each curve has been tted by

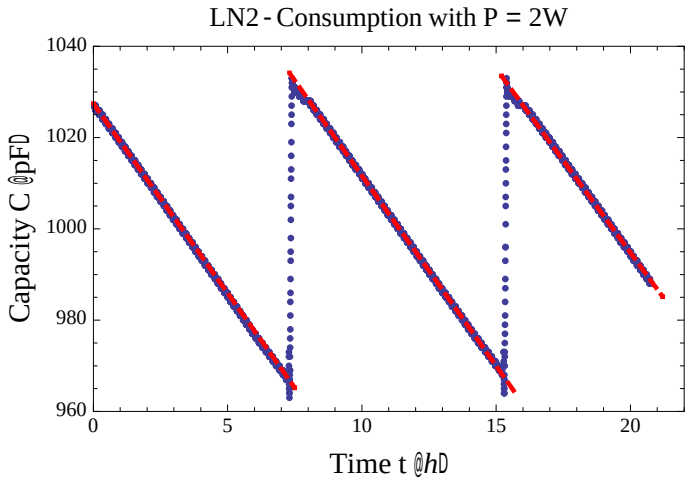

Figure 4.11: LN_2-consumption for $P = 2\,W$. The three slopes result from the lling-system, which lls the detector every 8 h. The red dashed lines indicate the linear t to each curve.

a linear regression: $C = m_C \quad t + b_C$ therefore three values of $m_{i;C}$ are obtained with an average:

$$m_C = \frac{1}{3} \sum_{i=1}^{3} m_{i;C} \tag{4.14}$$

and its standard deviation. This causes the consumption:

$$= \frac{m_C}{C} \quad 4{:}5\,l \tag{4.15}$$

for one P-value. This has been repeated for several heating powers. At rst the power was increased in 0.5 W-steps until 3 W and after that in 1 W-steps until a maximum of 7 W. The curves of the other measurements are listed in appendix B. The measured consumption as a function of the applied heating loss is displayed in gure 4.12. As expected from equation 4.12, the consumption (P) is strictly linear in P. The tted function was found as:

$$(P) = (27{:}66 \quad 1{:}05) \quad 10^{\,3}\frac{l}{W\,h} \quad P + (0{:}241 \quad 0{:}004)\frac{l}{h} \tag{4.16}$$

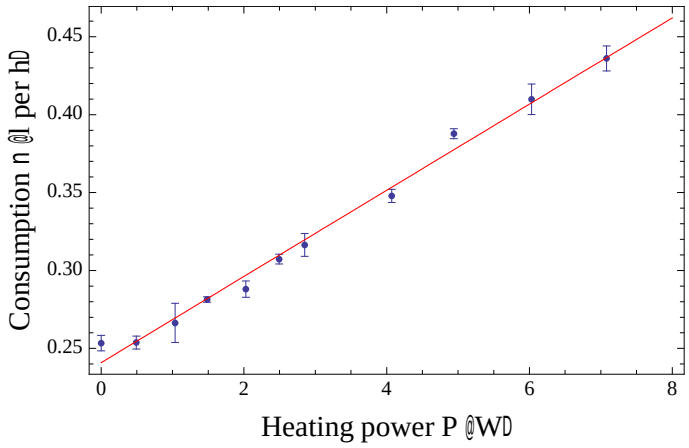

Figure 4.12: Results of the consumption-measurement with ATC(4). The consumption (P) is a linear function of the applied heating loss P.

The axis intercept $_0 = 0{:}241\frac{l}{h}$ is related to the cryostat with aluminium blocks inside but without any extra heating power applied. The consumption $_0$ di ers for each detector system, when the con guration of the cold part (e.g. cabeling, amount of crystals etc.) is di erent. Multiplying equation 4.16 with $Q_V \quad _{LN_2}$ leads to the consumption $_W$ expresses in Watt:

$$_W(P) = (1{:}23 \quad 0{:}05) \quad P + (10{:}73 \quad 0{:}18)\,W \tag{4.17}$$

According to equation 4.10 and 4.11, the consumption $_W$ is given by: $_W =$ $(P + P_0)$. Thus the factor measured in this experiment is given by: $= (1{:}23 \quad 0{:}05)$. This result is surprising, since is larger than 1 which means more heating power than produced by the caddock is injected into the cooling nger. This is only reasonable if a thermal radiation emitted from another source inside the cryostat is considered.

Chapter 5

The LN_2-read-out (II): A capacitive preamplifier

Up to now all capacitive measurements were performed by measuring the filling capacity directly with a multimeter which was read out by a PC. Since the variations of the measured capacities are $\pm 2\,\%$, a high accuracy of the read out is needed. This implies that the read-out-device itself does not influence the measuring capacity. Measuring device (I) however does not fulfill this condition, because the BNC-cable which links the multimeter with the capacitive read-out of the dewar has an own capacity C_{BNC} = 150 pF. This capacity is in the same range as the variation between C_{min} and C_{max}. Moreover the measured capacity is shifted by C_{BNC} with respect to the real filling capacity of the system. Apart from this, the measured capacity is also influenced by the adjusted measuring-range of the multimeter. Figure 5.1 shows a capacitve measurement which has been performed with measuring device (I). The two horizontal lines (marked by red circles) refer to capacity values which have not been measured but written by the program which reads out the multimeter. Thus all measured data which has been taken with device (I) has to be corrected by those unwanted values.

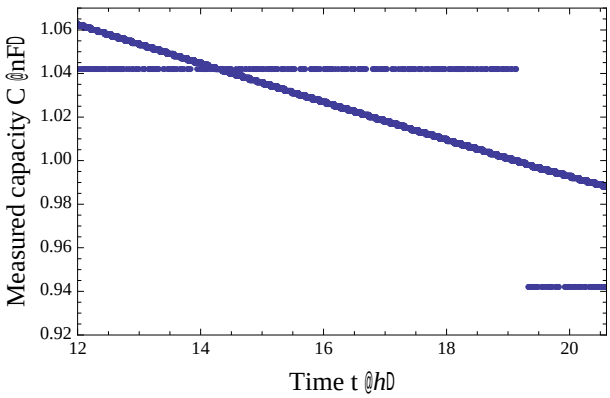

Figure 5.1: Result of a capacitive measurement with ATC(2). The measured capacity C runs linear with respect to the time t. The horizontal data-points which are marked with red circles do not refer to the measured capacity, as they result from the PC-read-out-software. The program wrote frequently some extra capacity values of C = 1042 pF and C = 942 pF into the measured data.

In order to avoid all these problems a LN_2-read-out-device is needed which meets the following conditions:

Measuring the capacity C and amplifying it

Converting the measuring capacity into a signal which can be easily read

out and is independent of further read-out-devices (e.g. BNC-cabling, range of multimeter)

Sensitive to capacity changes in the range of 12 %

Compact in size

The device should be supplied with the warm and cold ampli er's low voltage

A DC-operator, such that the detector electronics is not disturbed by measuring the capacity C

Such a device has been developed by Gheorghe Pascovici and is realised by a capacitive preampli er.

5.1 The capacitive preampli er

The basic principle of the LN_2-read-out-device (II) is measuring the di erence C between the measuring capacity C_m and a xed reference capacity C_r, instead of measuring the lling capacity C_m over the full range of 1000 pF. Thus this device is more sensitive to small changes of C_m which are typically about 12 %. The reference capacity C_r has been set to $C_r = \frac{1}{2}(C_{m;max} + C_{m;min})$, as $C_{m;max}$ is the measured maximum lling capacity and $C_{m;min}$ the minimum capacity respectively.

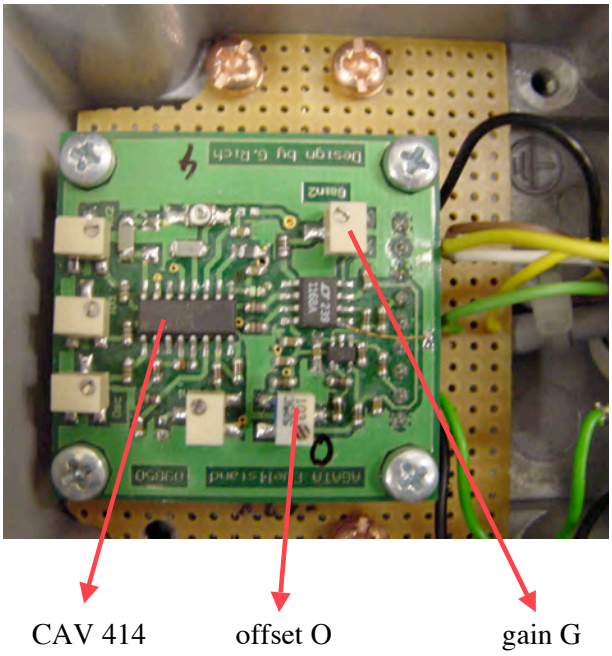

Figure 5.2: Capacitive LN_2-read-out-device developed by the electronic workshop at IKP Cologne. The CAV 414 converts the measuring capacity into a voltage. The gain G and o set O of the nal output signal are adjustable.

The output signal of the LN_2-read-out-device is a direct-voltage signal which can be manipulated by an adjustable gain G and o set O (see g. 5.2) and therefore set to de ned values. Figure 5.2 shows a photograph of the LN_2-read-out-device which converts the measuring capacity C_m into a voltage U_m. The circuit diagram of this device is displayed in g. 5.3. The conversion of the lling capacity into a DC-voltage is predominantly done by an analogue measuring device called CAV414 (developed by Analog Microelectronics). The working principle of this device can be seen on [Gmb08] in detail. But the main and basic aspects are discussed in the following section.

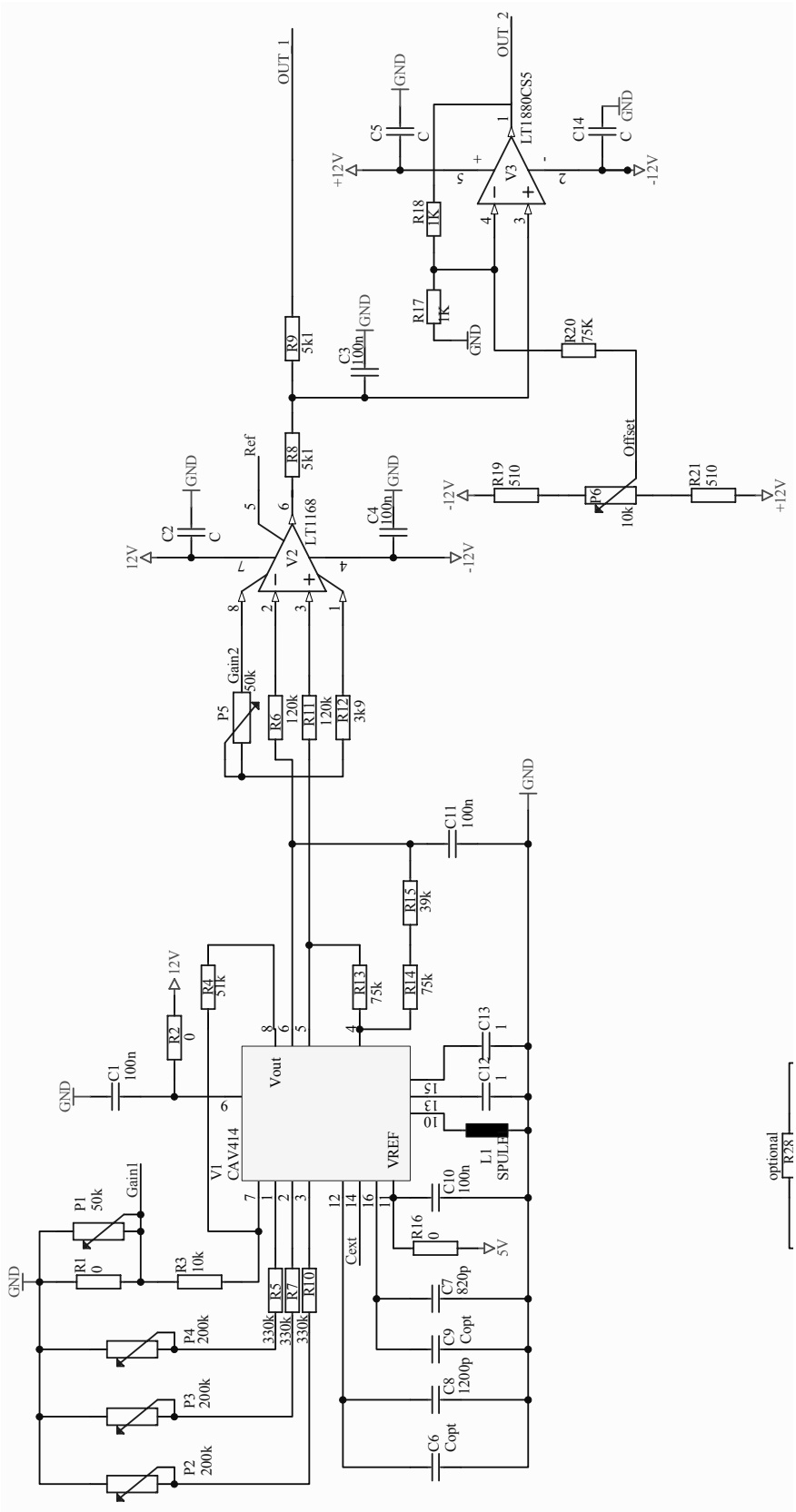

Figure 5.3: Circuit diagram of the LN_2-read-out-device designed at IKP Cologne. The potentiometer P5 (Gain 2) and P6 (O set) are the adjustable gain and o set as shown in g. 5.2.

5.1.1 The CAV414

The CAV414 is a capacity/voltage transducer with an adjustable output voltage. A reference oscillator drives two identical integrators, as one is equipped with the reference capacity C_r and the other one with the measuring capacity C_m respectively (see g. 5.4). The output signals of each integrator are subtracted from each other, as their amplitude depends on C_r and C_m respectively. This di erence signal is ltered and ampli ed several times so that the output signal is a DC voltage which is proportional to $C = C_m \quad C_r$ [Gmb08]. A triangular wave oscillator is in principle realised by the combination of a

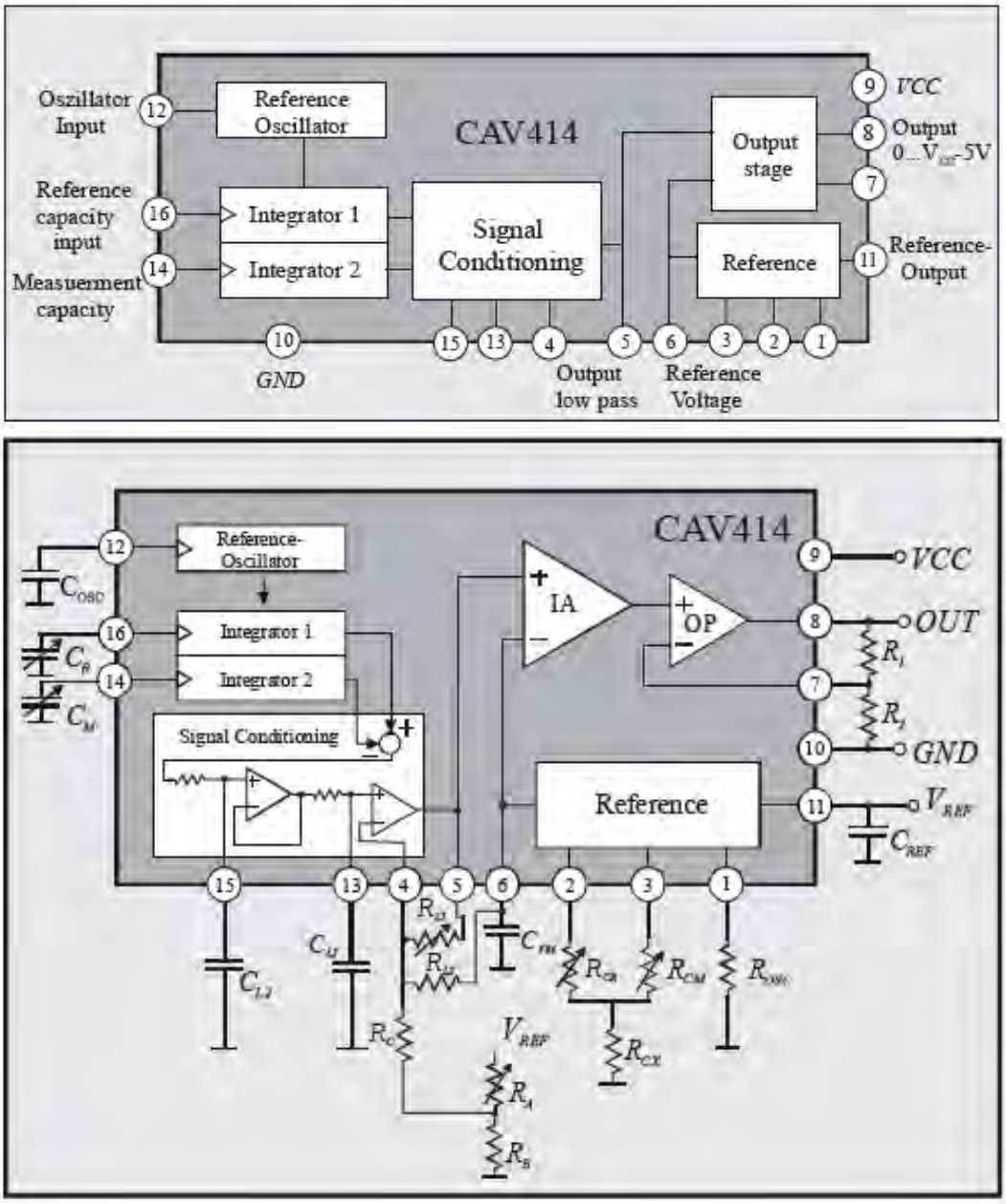

Figure 5.4: Top: Working principle of the CAV414 [Gmb08]. Bottom: Functional diagram of the CAV414 for a constant oscillator frequency f_{osc} = const [Gmb08].

Schmitt Trigger and an Integrator. Since the lling capacity C_m is measured with respect to the cryostats ground, this method is not favourable. For this reason the oscillator used here consists of a constant current source which

charges/ discharges a grounded capacitor C by the constant currents $+I$ / $-I$ (see g. 5.5). If the capacitor is directly charged by the constant current I

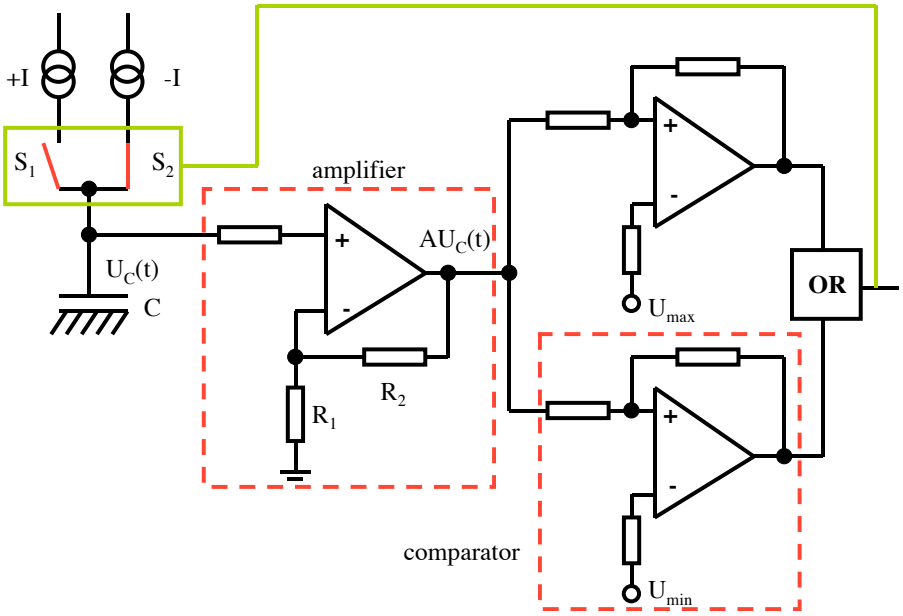

Figure 5.5: Simpli ed circuit-diagram of an oscillator (design by G.Pascovici).

for example, the voltage $U_C(t)$ after a time t at the capacitor is given by:

$$U_C(t) = \frac{1}{C} \quad Q(t) = \quad \frac{1}{C} \quad I \quad t \tag{5.1}$$

The voltage decreases linearly as a function of time t. This voltage signal passes a non-inverting ampli er and is ampli ed by the factor $A = \quad 1 + \frac{R_2}{R_1}$. The output $A \quad U(t)$ is injected into two identical comparators with di erent threshold-voltages U_{min} and U_{max}. A comparator switches between two xed voltages U_0 depending on the polarity of the di erence-signal $U_{in} \quad U_{trsh}$ as U_{trsh} is the threshold-voltage. A positive polarity of $U_{in} \quad U_{trsh}$ leads to $+U_0$ whereas a negative polarity leads to U_0 [EH05]. The lower comparator in g. 5.5 switches if the input voltage is $AU_C(t) < U_{min}$, whereas the upper comparator switches for $AU_C(t) > U_{max}$. Both comparator signals drive through an OR-gatter the switches S_1 and S_2. Considering the example displayed in g. 5.5, switch S_2 opens if $AU_C(t)$ is below U_{min} and the switch S_1 is closed. The capacitor is now charged by $+I$. If $U_C(t)$ exceeds U_{max}, switch S_1 is opened and S_2 closed respectively. The output signal of such a device is a triangular wave (see diagram a) of gure 5.6). The frequency of this signal is found by using equation 5.1:

$$U_{max} \quad = \quad \frac{1}{C} \quad I \quad \frac{T}{2} + U_{min} \quad , \tag{5.2}$$

$$f \quad = \quad \frac{I}{2 \quad (U_{max} \quad U_{min}) \quad C} \tag{5.3}$$

Thus the frequency f_{osc} of the reference oscillator is determined by its capacity C_{osc} and the constant current I_{osc}. The two integrators are working in much the same way as the reference oscillator (see g. 5.5), whereas the integrators are not equipped with two comparators (like the oscillator in g. 5.5). The

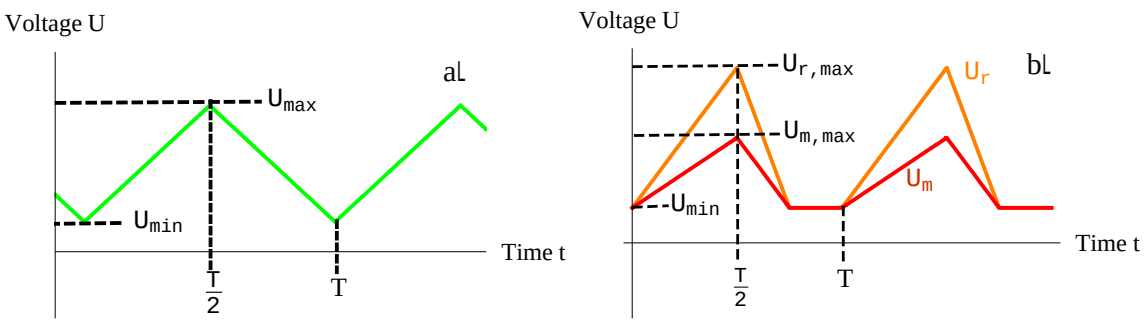

Figure 5.6: a) Output signal of the reference oscillator with period T, maximum amplitude U_{max} and minimum amplitude U_{min}. b) Output signals U_r and U_m of the two integrators which have the same period T as the reference oscillator.

constant current sources of each integrator is driven phase locked and clock synchronised by the reference oscillator instead [Gmb08]. This feature ensures that the output signals of both integrators are not shifted to each other and have exactly the same frequency. Another characteristic of the integrators is that the discharging current is twice of the charging current. Thus the ratio between the charging time t_{charge} and discharging time $t_{discharge}$ of the capacitor is given by: $t_{charge} = 2 \quad t_{discharge}$ [Gmb08]. The minimum voltage of each integrator is set to a xed value of $U_{min} = 1:2\,V$ [Gmb08]. The maximum output voltages of both integrators are given by:

$$U_{m;max} = \frac{I_m}{2 \quad f_{osc} \quad C_m} \tag{5.4}$$

$$U_{r;max} = \frac{I_r}{2 \quad f_{osc} \quad C_r} \tag{5.5}$$

I_m is the charging current of the integrator with capacity C_m and I_r the charging current of the integrator with C_r respectively. Diagram b) of g. 5.6 displays the output signals of the integrators. In a next step both triangular signals U_r and U_m are subtracted from each other which leads to the di erence signal $U_{rm} = U_r \quad U_m$. This signal is ltered by an active lowpass and ampli ed (see g. 5.4) which leads to the DC-signal U_{LPOUT} at pin no. 5 [Gmb08]:

$$U_{LPOUT} = 1 + \frac{R_{L1}}{R_{L2}} \quad \frac{3}{8} \quad U_{rm;filtered} \tag{5.6}$$

The DC-voltage U_M at pin 6 (pin out of the CAV414 see appendix C) is subtracted from equation 5.6: $U_{LPOUT} \quad U_M$. This signal is ampli ed by an instrumentation and operational ampli er (see functional diagram in g. 5.4). The instrumental ampli er has a xed gain $G = 5$, whereas the gain of the operational ampli er is determined by the two resistors R_1 and R_2. This leads to the output voltage [Gmb08]:

$$U_{out} = 5 \quad 1 + \frac{R_1}{R_2} \quad \overset{h}{U_{LPout}} \quad \overset{i}{U_M} \; / \; C_m \quad C_r \tag{5.7}$$

The resistors R_1, R_2, R_{L1} and R_{L2} are adjustable and change the amplitude of U_{out}. U_M is an adjustable DC-potential. Considering the circuit diagram shown in g. 5.3 the resistors R_{L1} and R_{L2} are realised by $R_{L1} = 75\,k$ and $R_{L2} = (75 + 39)\,k$. The ampli cation through the resistors R_1 and R_2 is

realised in the circuit diagram by the potentiometer P1, the resistor R3 and R4.
The CAV414 might be operated in two di erent con gurations [Gmb08]:

1. The load currents I_r and I_m are selected as constant, thus the oscillator frequency f_{osc} has to be adjusted.

2. The oscillator frequency f_{osc} is constant and the load currents I_r and I_m are functions of the resistors R_{CM} and R_{CR}.

The second method is realised in the LN_2-read-out-device, since the potentiometers P2, P3 and P4 are used for adjusting the currents I_r, I_m and I_{osc}.

5.1.2 Further signal processing

The circuit diagram in g. 5.3 shows that the output voltage U_{out} of the CAV414 is connected to pin 7 (as indicated by the functional diagram) but not read out. Instead of that, the voltages U_{LPOUT} and U_M are plugged into an instrumentation ampli er namely LT1168.
The pin out of this device is shown in g. 5.7. The voltages U_{LPOUT} and U_M are connected to pin 2 and 3. The resistor R_G is realised by the resistor R12 and the potentiometer P5 (Gain 2) as shown in the circuit diagram. The nal output gain is given by [Tec00]: $G = (49.4\,k\Omega/R_G) + 1 = (49.4\,k\Omega/(R12 + R_{P5}) + 1$. This adjustable gain is indicated by the black circle in g. 5.2. In a last step, the output voltage of the LT1168 is connected to a non-inverting ampli er (LT1880CS5). The inverting input of this device is connected to an adjustable o set-voltage (potentiometer P6 in g. 5.3). This adjustable o set is also indicated by a black circle in g. 5.2. The nal output voltage of the LN_2-read-out-device is taken at the output OUT 2 and is a function of the measuring capacity C_m, the gain G (adjusted by potentiometer P5) and the o set O (potentiometer P6).

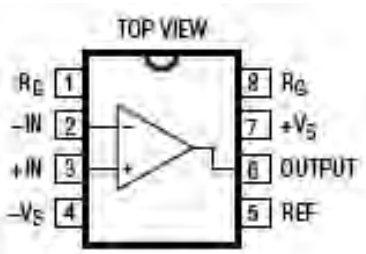

Figure 5.7: Pin out of the LT1168 instrumentation ampli er. The output gain of this ampli er is determined by only one external resistor R_G [Tec00].

5.1.3 First tests with the prototype

A rst prototype of a LN_2-read-out-device (see g. 5.8) has been tested at ATC(4) being in vertical position. The results of this measurement are displayed in diagram a) of g. 5.8. The slope of the measured curve is not linear in time as expected. The capacity C_{BNC} of the BNC-cable was not considered when adjusting the measuring range of the prototype therefore the device is not detecting the lling capacity in a proper way. Nevertheless the LN_2-read-out-device is working since the curve in diagram a) is linear for capacities which are in the range of 780 880 pF. Diagram b) in g. 5.8 shows a plot of the device-output versus the lling capacity which has been corrected by C_{BNC}. The red curve in this diagram is a linear regression $U(C) = m\ C + b$ through the data points. The prototype was also used for a position-dependent

Figure 5.8: a) Results of the lling capacity measurement at ATC(4) performed with a prototype of the LN_2-read-out device. b) Plot of the devices output U versus the measuring capacity C of ATC(4). The red line is a linear regression U(C) = mC + b through the measured data. Down left: Photo of the prototype which is equipped with an BNC-input, an SMB-outbut and a voltage supply. Gain and o set of the device are adjustable by two potentiometers. Down right: ATC(4) inclined by the angle = 45 . The read-out-device is xed onto the dewar. The results of this measurement are shown and discussed in chapter 6.